

New physics footprints in the angular distribution of $B_s \rightarrow D_s^*(\rightarrow D_s\gamma, D_s\pi)\tau\nu$ decays

Nilakshi Das* and Rupak Dutta†

National Institute of Technology Silchar, Silchar 788010, India

Hints of lepton flavor universality violation observed in various flavor ratios such as R_D , R_{D^*} , $R_{J/\psi}$, $P_\tau^{D^*}$ and $F_L^{D^*}$ in $B \rightarrow D^{(*)}\ell\nu$ and $B_c \rightarrow J/\psi\ell\nu$ charge current decays have opened new avenues to search for indirect evidences of beyond the standard model physics. Motivated by these anomalies, we perform a detailed angular analysis of $B_s \rightarrow D_s^*(\rightarrow D_s\gamma, D_s\pi)\ell\nu$ decays that proceed via similar $b \rightarrow c\ell\nu$ quark level transition. We use the most general effective Hamiltonian for $b \rightarrow c\ell\nu$ process and give predictions of several q^2 and $\cos\theta$ dependent observables for the $B_s \rightarrow D_s^*(\rightarrow D_s\gamma, D_s\pi)\ell\nu$ decays in the standard model and in the presence of various real and complex new physics couplings. The results pertaining to this decay are competent to address the anomalies in the charge current sector.

PACS numbers: 14.40.Nd, 13.20.He, 13.20.-v

I. INTRODUCTION

Lepton flavor universality that treats the three generations of charged leptons (e, μ, τ) to be identical except the differences in their masses in the weak decays of flavor changing processes has exposed the possibility of new physics (NP) which lies beyond the Standard Model (SM). The hunt of new physics lies not just at the frontiers of the lepton flavor violating decays at the collider experiments but also in various other phenomena such as matter-antimatter asymmetry of the universe, dark matter, neutrino mass, mass hierarchy problem and so on. The B factories, since their inception, have been instrumental in exploring NP. The B factories have literally witnessed the breaking of lepton flavor universality in $b \rightarrow c\ell\nu$ charged current and $b \rightarrow sl^+l^-$ neutral current transition decays. Although the results of several decay modes revealed the signature of lepton flavor universality violation, none of them are statistically significant to account for the evidence of new physics. The future upgradation of LHC with improved precision and with more number of new measurements can reduce the systematic error in the existing measurements and at the same time the efforts to study various similar decay modes eventually add up to tackle the possible new physics puzzle in semileptonic B decays. In the present context, we limit ourself to discuss the anomalies in the $b \rightarrow c\ell\nu$ charged current quark level transitions.

- **Anomalies in R_D :** The ratio of branching ratio R_D for the decay mode $B \rightarrow D\ell\nu$ is defined as

$$R_D = \frac{\mathcal{B}(B \rightarrow D\tau\nu_\tau)}{\mathcal{B}(B \rightarrow D\{e/\mu\}\nu_{(e/\mu)})}. \quad (1)$$

A very precise SM prediction of $R_D = 0.299 \pm 0.003$ and $R_{D^*} = 0.300 \pm 0.008$ [1–6] was reported using the $B \rightarrow D$ form factors obtained in lattice QCD approach. In 2016, FLAG working group predicated the most accurate SM results of $R_D = 0.300 \pm 0.008$ by combining two lattice QCD results with the experimental form factor of $B \rightarrow D\ell\nu$ obtained from BABAR (2010) [7] and BELLE (2016) [8]. In 2012, for the first time BABAR collaboration experimentally measured the value of the ratio of branching to be $R_D = 0.440 \pm 0.058 \pm 0.042$ [9]. This measurement was found to be deviated from the theoretical prediction at 2.6σ level. Later, BELLE collaboration in 2015 [10] measured the value to be $R_D = 0.375 \pm 0.064 \pm 0.026$. Similarly in the Mariond 2019, the BELLE collaboration announced the updated measurement in R_D and reported it to be $R_D = 0.307 \pm 0.037 \pm 0.016$ [11]. Although it is consistent with its previous measurement, the average of all the three measurements obtained from the HFLAV still deviates at 1.4σ from the SM expectation [1–6]. Although the deviation from the SM prediction is decreased from 2.6σ to 1.4σ , the tension between theory and experiment still exists.

*Electronic address: nilakshi_rs@phy.nits.ac.in

†Electronic address: rupak@phy.nits.ac.in

- **Anomalies in R_{D^*} :** The ratio of branching ratio R_{D^*} for the decay mode $B \rightarrow D^* l \nu$ is defined as

$$R_{D^*} = \frac{\mathcal{B}(B \rightarrow D^* \tau \nu_\tau)}{\mathcal{B}(B \rightarrow D^* \{e/\mu\} \nu_{(e/\mu)})}. \quad (2)$$

The first SM prediction of $R_{D^*} = 0.252 \pm 0.003$ was reported in Ref. [12]. Several New calculations have become available since 2017 [5, 6, 13]. Although there are differences in the evaluation of the theoretical uncertainty, all the new calculations are found to be in very good agreement with each other. They are more robust and are consistent with the old predictions for R_{D^*} as well. The arithmetic average obtained by HFLAV is $R_{D^*} = 0.258 \pm 0.005$ [5, 6, 13]. As of $B \rightarrow D^*$ lattice QCD form factors are concerned, at present only some unquenched calculations at the zero recoil exists from the Fermilab Lattice and MILC Collaborations [14, 15]. The non zero recoil calculations for the $B \rightarrow D^*$ form factors are limited by the availability of computational resources and the efficient algorithms. First experimental measurement of $R_{D^*} = 0.332 \pm 0.024 \pm 0.018$ was reported by BABAR collaboration [16] and it was found to be deviated at 2.7σ from the SM prediction. Later in 2015, 2016 and 2017, BELLE collaboration measured the value of R_{D^*} to be $0.293 \pm 0.038 \pm 0.015$ [10], $0.302 \pm 0.030 \pm 0.011$ [17] and $0.270 \pm 0.035^{+0.028}_{-0.025}$ [18], respectively. Similarly, in the year 2015 and 2017, LHCb collaboration also measured the value of R_{D^*} to be $0.336 \pm 0.027 \pm 0.030$ [19] and $0.291 \pm 0.019 \pm 0.029$ [20], respectively. The recent update of R_{D^*} measurement from the BELLE collaboration [21] announced in the Mariond 2019 is $R_{D^*} = 0.283 \pm 0.018 \pm 0.014$. At present, the average of various measurements of R_{D^*} from HFLAV still deviates from the SM expectation at the level of 2.5σ .

- **Anomalies in $R_{J/\psi}$:** The ratio of branching ratio $R_{J/\psi}$ for the decay mode $B_c \rightarrow J/\psi l \nu$ is defined as

$$R_{J/\psi} = \frac{\mathcal{B}(B_c \rightarrow J/\psi \tau \bar{\nu}_\tau)}{\mathcal{B}(B_c \rightarrow J/\psi \{e/\mu\} \bar{\nu}_{(e/\mu)})}. \quad (3)$$

The SM prediction of $R_{J/\psi}$ can be found in the Refs. [22–28]. In addition, the authors in Ref. [29] provide the SM bound to be $R_{J/\psi} \in [0.20, 0.39]$ at 95% confidence level. Very recently, the HPQCD collaboration reported the first lattice QCD results of $R_{J/\psi}$ and reported it to be 0.2582 ± 0.0038 [30]. The experimental measurement of $R_{J/\psi}$ from the LHCb collaboration in 2017 has reported the value of $R_{J/\psi} = 0.71 \pm 0.17 \pm 0.18$. This measurement of $R_{J/\psi}$ deviates from the SM prediction at 1.8σ level.

- **Anomalies in $P_\tau^{D^*}$ and $F_L^{D^*}$:** The τ polarization fraction and the longitudinal polarization fraction of D^* meson in $B \rightarrow D^* \tau \nu$ decays are defined as

$$P_\tau^{D^*} = \frac{\Gamma^+(B \rightarrow D^* \tau \bar{\nu}_\tau) - \Gamma^-(B \rightarrow D^* \tau \bar{\nu}_\tau)}{\Gamma(B \rightarrow D^* \tau \bar{\nu}_\tau)}, \quad F_L^{D^*} = \frac{\Gamma(B \rightarrow D_L^* \tau \bar{\nu}_\tau)}{\Gamma(B \rightarrow D^* \tau \bar{\nu}_\tau)}. \quad (4)$$

The measured value of the τ polarization fraction $P_\tau^{D^*} = -0.38 \pm 0.51^{+0.21}_{-0.16}$ [31, 32] deviates from the SM prediction of 0.497 ± 0.013 [33] at 1.6σ level. Similarly, for $F_L^{D^*}$, the measured value $F_L^{D^*} = 0.60 \pm 0.08 \pm 0.035$ [34] deviates from the SM expectation of 0.46 ± 0.04 [35] at 1.5σ level.

So far till date there have been several model independent and model dependent NP analysis on $b \rightarrow cl\nu$ decays. We report here an incomplete list of various literature [36–77]. Recently, in Ref. [78, 79], the authors calculate the best fit values of vector, scalar and tensor NP couplings in $1D$ and $2D$ scenarios by fitting the experimental measurements of $R_{D^{(*)}}$, $P_\tau^{D^*}$ and $F_L^{D^*}$ by considering the correlation between the observable $R_D - R_{D^*}$. Similarly, in Ref [60], the authors obtained the best fit values of NP Wilson coefficients (WC) by considering the experimental values of $R_D - R_{D^*}$ in a bayesian statistical approach assuming complex NP WCs. Moreover, in Ref [80], the authors perform a global fit of NP WCs by considering $R_{D^{(*)}}$, $P_\tau^{D^*}$, $F_L^{D^*}$ and differential q^2 distribution of $B \rightarrow D\tau\nu$ and $B \rightarrow D^*\tau\nu$ decays. In addition the authors consider the constraints coming from the branching fraction of $B_c \rightarrow \tau\bar{\nu}_\tau$ decays.

The SM analysis of $B_s \rightarrow D_s^* l \nu$ decays has been performed by several authors using the form factors obtained in the constituent quark meson (CQM) model [81], the QCD sum rule [82, 83], the light cone sum rule (LCSR) [84, 85], the covariant light-front quark model (CLFQM) [86], the instantaneous Bethe-Salpeter equation [87, 88], the lattice QCD at zero recoil point [89], the perturbative QCD approach [90, 91], the BGL parameterization of lattice QCD data. [92] and the relativistic quark model (RQM) based on the quasi-potential approach [93]. In Ref. [94], the authors perform a model independent analysis of NP effects in $B_s \rightarrow D_s^* l \nu$ decays by using the RQM form factors of Ref. [93]. They, however, treat D_s^* meson to be stable and did not consider any further decay of D_s^* to $D_s\gamma$ or $D_s\pi$.

In the present paper, we use the most general effective Lagrangian in the presence of NP and perform a detail angular analysis of $B_s \rightarrow D_s^*(\rightarrow D_s\gamma, D_s\pi) l \nu$ decays using the lattice QCD form factor results in the full q^2 range.

Among the two decay channels, the probability of D_s^* going to $D_s\gamma$ is 93%, whereas, for $D_s^* \rightarrow D_s\pi$, it is 5%. In this analysis we treat the NP WCs to be both real and complex. We give prediction of the branching fraction, longitudinal polarization fraction of D_s^* meson, forward backward asymmetry and several angular observables pertinent to $B_s \rightarrow D_s^*(\rightarrow D_s\gamma, D_s\pi)l\nu$ decays.

Study of this decay channel is well motivated for several reasons. From the experimental point of view, very recently, LHCb collaboration has provided a complementary information regarding the CKM matrix element V_{cb} using this decay channel. Similarly, LHCb collaboration has also reported the measured shape of the normalized differential decay distribution with respect to q^2 . It will allow to make a direct comparison between the experimental measurements with its theoretical values. Moreover, BELLE collaboration is accumulating large data samples which will help in measuring the branching fractions to a very good precision. A total of $(6.53 \pm 0.66) \times 10^6$ $B_s \bar{B}_s$ pair is obtained at the BELLE detector [95, 96] at electron-positron collider KEKB asymmetric energy. In BELLE-II the statistics will be increased by a factor of 40, and in the next decade the data are expected to be more than 50 times. Hence a precise measurement of observables pertaining to $B_s \rightarrow D_s^*l\nu$ decays may be feasible in near future which eventually will be crucial to reveal the evidence of lepton flavor universality violation in B meson decays. At the same time, from theoretical point of view, very recently in 2021, first lattice QCD results for $B_s \rightarrow D_s^*$ form factors have been reported by the HPQCD collaboration [98]. From the lattice QCD point of view, the $B_s \rightarrow D_s^*$ form factors have an advantage over the $B \rightarrow D^*$ form factors mainly for two reasons. First, the $B_s \rightarrow D_s^*$ does not contain the valence u/d quarks. Secondly, the D_s^* meson can be treated as stable as there is no Zweig-allowed strong two body decays because of its very narrow width.

This paper is organized as follows. In section II, we start with the most general effective weak Lagrangian for $b \rightarrow cl\nu$ decays in the presence of vector, scalar and tensor NP operators. We also report the relevant formula for all the observables pertaining to $B_s \rightarrow D_s^*(\rightarrow D_s\gamma, D_s\pi)l\nu$ decays in section II. In section III, We discuss the results obtained in the SM and in the presence of three different NP scenarios. Finally, we conclude with a brief summary of our results in section IV.

II. THEORETICAL FRAMEWORK

In the presence of NP, the effective weak Lagrangian for the $b \rightarrow cl\nu$ transition decays at renormalization scale $\mu = m_b$, can be written as [99, 100]

$$\begin{aligned} \mathcal{L}_{\text{eff}} = & -\frac{4G_F}{\sqrt{2}} V_{cb} \left\{ (1 + g_{V_L}) \bar{l}_L \gamma_\mu \nu_L \bar{c}_L \gamma^\mu b_L + g_{V_R} \bar{l}_L \gamma_\mu \nu_L \bar{c}_R \gamma^\mu b_R \right. \\ & \left. + g_{S_L} \bar{l}_R \nu_L \bar{c}_R b_L + g_{S_R} \bar{l}_R \nu_L \bar{c}_L b_R + g_{T_L} \bar{l}_R \sigma_{\mu\nu} \nu_L \bar{c}_R \sigma^{\mu\nu} b_L \right\} + \text{h.c.}, \end{aligned} \quad (5)$$

where, G_F is the Fermi coupling constant and V_{cb} is the Cabibbo kobayashi Maskawa (CKM) matrix element. The vector, scalar, and tensor type NP interactions denoted by $g_{V_{L,R}}$, $g_{S_{L,R}}$, and g_{T_L} NP couplings are associated with left handed neutrinos. We have not considered the right handed neutrino interactions in our analysis.

A. Angular decay distribution of $B_s \rightarrow D_s^*(\rightarrow D_s\gamma)l\nu$ decay mode

The four body differential decay distribution for the $B_s \rightarrow D_s^*(\rightarrow D_s\gamma)l\nu$ decay can be expressed in terms of the angular coefficients as [101]

$$\begin{aligned} \frac{d^4\Gamma(B \rightarrow D_s^*(\rightarrow D_s\gamma)l\nu)}{dq^2 d\cos\theta_l d\cos\theta_{D_s} d\phi} = & \mathcal{N}_\gamma P_{D_s^*} \left(1 - \frac{m_l^2}{q^2}\right)^2 \left\{ I_{1s} \sin^2\theta_{D_s} + I_{1c}(3 + \cos 2\theta_{D_s}) + (I_{2s} \sin^2\theta_{D_s} + I_{2c}(3 + \right. \\ & \left. \cos 2\theta_{D_s}) \cos 2\theta_l + I_3 \sin^2\theta_{D_s} \sin^2\theta_l \cos 2\phi + I_4 \sin 2\theta_{D_s} \sin 2\theta_l \cos \phi + I_5 \right. \\ & \left. \sin 2\theta_{D_s} \sin \theta_l \cos \phi + (I_{6s} \sin^2\theta_{D_s} + I_{6c}(3 + \cos 2\theta_{D_s}) \cos \theta_l) + I_7 \sin 2\theta_{D_s} \right. \\ & \left. \sin \theta_l \sin \phi + I_8 \sin 2\theta_{D_s} \sin 2\theta_l \sin \phi + I_9 \sin^2\theta_{D_s} \sin^2\theta_l \sin 2\phi \right\}, \end{aligned} \quad (6)$$

where the three momentum vector of the D_s^* meson and the normalization constant are defined as

$$|p_{D_s^*}| = \sqrt{\lambda(m_{B_s}^2, m_{D_s^*}^2, q^2)}/2m_{B_s}, \quad \mathcal{N}_\gamma = \frac{3G_F^2 |V_{cb}^2| \mathcal{B}(D_s^* \rightarrow D_s\gamma)}{128 (2\pi)^4 m_{B_s}^2}. \quad (7)$$

In the presence of vector, scalar and tensor NP couplings, the angular coefficients I_i , where $i = 1, \dots, 6$, can be expressed as \square

$$I_i = |1 + \epsilon_V|^2 I_i^{SM} + |\epsilon_R|^2 I_i^{NP,R} + |\epsilon_P|^2 I_i^{NP,T} + 2 \operatorname{Re}[\epsilon_R(1 + \epsilon_V^*)] I_i^{INT,R} + 2 \operatorname{Re}[\epsilon_P(1 + \epsilon_V^*)] I_i^{INT,P} + 2 \operatorname{Re}[\epsilon_T(1 + \epsilon_V^*)] I_i^{INT,T} + 2 \operatorname{Re}[\epsilon_R \epsilon_T^*] I_i^{INT,RT} + 2 \operatorname{Re}[\epsilon_P \epsilon_T^*] I_i^{INT,PT} + 2 \operatorname{Re}[\epsilon_P \epsilon_R^*] I_i^{INT,PR}. \quad (8)$$

Similarly, the angular coefficients I_7 , I_8 and I_9 can be written as

$$I_7 = 2 \operatorname{Im}[\epsilon_R(1 + \epsilon_V^*)] I_7^{INT,R} + 2 \operatorname{Im}[\epsilon_P(1 + \epsilon_V^*)] I_7^{INT,P} + 2 \operatorname{Im}[\epsilon_T(1 + \epsilon_V^*)] I_7^{INT,T} + 2 \operatorname{Im}[\epsilon_R \epsilon_T^*] I_7^{INT,RT} + 2 \operatorname{Im}[\epsilon_P \epsilon_T^*] I_7^{INT,PT} + 2 \operatorname{Im}[\epsilon_P \epsilon_R^*] I_7^{INT,PR}, \\ I_{(8/9)} = 2 \operatorname{Im}[\epsilon_R(1 + \epsilon_V^*)] I_{(8/9)}^{INT,R}, \quad (9)$$

where

$$\epsilon_V = g_{V_L}, \quad \epsilon_R = g_{V_R}, \quad \epsilon_P = g_{S_R} - g_{S_L} \quad \epsilon_S = g_{S_R} + g_{S_L} \quad \epsilon_T = g_{T_L}. \quad (10)$$

Here I_i^{SM} represents the angular coefficients in the SM and all other terms correspond to NP, interference of NP with NP, and interference of SM with NP, respectively. We refer to Ref [101] for all the omitted details.

1. The q^2 dependent observables

We define several q^2 dependent observables for the $B_s \rightarrow D_s^*(\rightarrow D_s \gamma) l \nu$ decay mode.

- The differential branching ratio, the lepton forward-backward asymmetry $A_{FB}^l(q^2)$, the forward-backward Asymmetry of transversely polarized D_s^* meson $A_{FB}^T(q^2)$ and the convexity parameter $C_F^l(q^2)$ are defined as [60]

$$\frac{d\Gamma}{dq^2}(q^2) = \mathcal{N}_\gamma |\vec{P}_{D_s^*}| \left(1 - \frac{m_l^2}{q^2}\right)^2 \frac{16}{9} \pi \left(3I_{1S} + 12I_{1c} - I_{2s} - 4I_{2c}\right), \\ A_{FB}^l(q^2) = \frac{8\pi}{3} \frac{\mathcal{N}_\gamma |\vec{P}_{D_s^*}| \left(1 - \frac{m_l^2}{q^2}\right)^2 (I_{6s} + 4I_{6c})}{d\Gamma/dq^2}, \quad A_{FB}^T(q^2) = \frac{32\pi}{3} \frac{\mathcal{N}_\gamma |\vec{P}_{D_s^*}| \left(1 - \frac{m_l^2}{q^2}\right)^2 I_{6c}}{d\Gamma_T/dq^2}, \\ F_L^{D_s^*}(q^2) = \frac{16\pi}{9} \frac{\mathcal{N}_\gamma |\vec{P}_{D_s^*}| \left(1 - \frac{m_l^2}{q^2}\right)^2 (3I_{1s} - I_{2s})}{d\Gamma/dq^2}, \quad C_F^l(q^2) = \frac{32\pi}{3} \frac{\mathcal{N}_\gamma |\vec{P}_{D_s^*}| \left(1 - \frac{m_l^2}{q^2}\right)^2 (I_{2s} + 4I_{2c})}{d\Gamma/dq^2} \quad (11)$$

- The angular observables $A_3(q^2)$, $A_4(q^2)$, $A_5(q^2)$, $A_{6s}(q^2)$, $A_7(q^2)$, $A_8(q^2)$ and $A_9(q^2)$ are defined as [60]

$$A_3(q^2) = \frac{16}{9} \frac{\mathcal{N}_\gamma |\vec{P}_{D_s^*}| \left(1 - \frac{m_l^2}{q^2}\right) I_3}{d\Gamma/dq^2}, \quad A_4(q^2) = -\frac{64}{9} \frac{\mathcal{N}_\gamma |\vec{P}_{D_s^*}| \left(1 - \frac{m_l^2}{q^2}\right) I_4}{d\Gamma/dq^2}, \\ A_5(q^2) = -\frac{8\pi}{3} \frac{\mathcal{N}_\gamma |\vec{P}_{D_s^*}| \left(1 - \frac{m_l^2}{q^2}\right) I_5}{d\Gamma/dq^2}, \quad A_{6s}(q^2) = -\frac{288\pi}{24} \frac{\mathcal{N}_\gamma |\vec{P}_{D_s^*}| \left(1 - \frac{m_l^2}{q^2}\right) I_{6s}}{d\Gamma/dq^2}, \\ A_7(q^2) = -\frac{8\pi}{3} \frac{\mathcal{N}_\gamma |\vec{P}_{D_s^*}| \left(1 - \frac{m_l^2}{q^2}\right) I_7}{d\Gamma/dq^2}, \quad A_8(q^2) = \frac{64}{9} \frac{\mathcal{N}_\gamma |\vec{P}_{D_s^*}| \left(1 - \frac{m_l^2}{q^2}\right) I_8}{d\Gamma/dq^2}, \\ A_9(q^2) = \frac{16}{9} \frac{\mathcal{N}_\gamma |\vec{P}_{D_s^*}| \left(1 - \frac{m_l^2}{q^2}\right) I_9}{d\Gamma/dq^2}. \quad (12)$$

- The ratio of branching fraction is defined as follows

$$R_{D_s^*}(q^2) = \frac{d\Gamma/dq^2|_{\tau\text{-mode}}}{d\Gamma/dq^2|_{e\text{-mode}}} \quad (13)$$

2. The $\cos \theta$ dependent observables

We also define several $\cos \theta_{D_s}$ and $\cos \theta_l$ dependent observables. They are

$$\begin{aligned}
F_L(\cos \theta_{D_s}) &= \frac{\mathcal{N}_\gamma |\vec{P}_{D_s^*}| \left(1 - \frac{m_l^2}{q^2}\right)^2 2\pi \int_{q_{min}^2}^{q_{max}^2} (2I_{1s} - \frac{2}{3}I_{2s})(1 - \cos^2 \theta_{D_s}) dq^2}{\Gamma(B_s \rightarrow D_s^*(\rightarrow D\gamma) l \nu)} \\
F_T(\cos \theta_{D_s}) &= \frac{\mathcal{N}_\gamma |\vec{P}_{D_s^*}| \left(1 - \frac{m_l^2}{q^2}\right)^2 4\pi \int_{q_{min}^2}^{q_{max}^2} (2I_{1c} - \frac{2}{3}I_{2c})(1 + \cos^2 \theta_{D_s}) dq^2}{\Gamma(B_s \rightarrow D_s^*(\rightarrow D\gamma) l \nu)} \\
F_L(\cos \theta_l) &= \frac{8\pi \mathcal{N}_\gamma |\vec{P}_{D_s^*}| \left(1 - \frac{m_l^2}{q^2}\right)^2 \int_{q_{min}^2}^{q_{max}^2} (I_{1s} + I_{2s}(2 \cos^2 \theta_l - 1) + I_{6s} \cos \theta_l) dq^2}{3 \Gamma(B_s \rightarrow D_s^*(\rightarrow D_s \gamma) l \nu)} \\
F_T(\cos \theta_l) &= \frac{32\pi \mathcal{N}_\gamma |\vec{P}_{D_s^*}| \left(1 - \frac{m_l^2}{q^2}\right)^2 \int_{q_{min}^2}^{q_{max}^2} (I_{1c} + I_{2c}(2 \cos^2 \theta_l - 1) + I_{6c} \cos \theta_l) dq^2}{3 \Gamma(B_s \rightarrow D_s^*(\rightarrow D_s \gamma) l \nu)} \\
A_{FB}^l(\cos \theta_{D_s}) &= \frac{\mathcal{N}_\gamma |\vec{P}_{D_s^*}| \left(1 - \frac{m_l^2}{q^2}\right)^2 2\pi \int_{q_{min}^2}^{q_{max}^2} [(I_{6s} + 2I_{6c}) + (2I_{6c} - I_{6s}) \cos^2 \theta_{D_s}] dq^2}{d\Gamma/d \cos \theta_{D_s}}, \tag{14}
\end{aligned}$$

where

$$\frac{d\Gamma}{d \cos \theta_{D_s}} = \frac{4\pi}{3} \int_{q_{min}^2}^{q_{max}^2} \mathcal{N}_\gamma |\vec{P}_{D_s^*}| \left(1 - \frac{m_l^2}{q^2}\right)^2 [(3I_{1s} - I_{2s} + 6I_{1c} - 2I_{2c}) + (I_{2s} - 3I_{1s} + 6I_{1c} - 2I_{2c}) \cos^2 \theta_{D_s}] dq^2$$

B. Angular decay distribution of $B_s \rightarrow D_s^*(\rightarrow D_s \pi) l \nu$ decay mode

Starting with the effective Lagrangian of Eq. 5, the four body differential decay distribution of $B_s \rightarrow D_s^*(\rightarrow D_s \pi) l \nu$ can be written as follows [60, 102].

$$\begin{aligned}
\frac{d^4\Gamma(B \rightarrow D_s^*(\rightarrow D_s \pi) l \nu)}{dq^2 d \cos \theta_l d \cos \theta_{D_s} d\phi} &= \frac{9}{32\pi} \left\{ I_{1s} \sin^2 \theta_{D_s} + I_{1c} \cos^2 \theta_{D_s} + (I_{2s} \sin^2 \theta_{D_s} + I_{2c} \cos^2 \theta_{D_s}) \cos 2\theta_l \right. \\
&\quad + (I_3 \cos 2\phi + I_9 \sin 2\phi) \sin^2 \theta_{D_s} \sin^2 \theta_l + (I_4 \cos \phi + I_8 \sin \phi) \sin 2\theta_{D_s} \sin 2\theta_l \\
&\quad \left. + (I_5 \cos \phi + I_7 \sin \phi) \sin 2\theta_{D_s} \sin \theta_l + (I_{6s} \sin^2 \theta_{D_s} + I_{6c} \cos^2 \theta_{D_s}) \cos \theta_l \right\}, \tag{15}
\end{aligned}$$

where the angular coefficients are [60, 102]

$$\begin{aligned}
I_{1c} &= N_F \left[2\left(1 + \frac{m_l^2}{q^2}\right) (\mathcal{A}_0 + 4|\mathcal{A}_{T0}|^2) - \frac{16m_l}{\sqrt{q^2}} \text{Re}[\mathcal{A}_0^L \mathcal{A}_{T0}^L] + \frac{4m_l^2}{q^2} |\mathcal{A}_{tP}|^2 \right] \\
I_{1s} &= N_F \left[\frac{1}{2} \left(3 + \frac{m_l^2}{q^2}\right) (|\mathcal{A}_\perp^L|^2 + |\mathcal{A}_\parallel^L|^2) + 2\left(1 + \frac{3m_l^2}{q^2}\right) (|\mathcal{A}_{T\perp}^L|^2 + |\mathcal{A}_{T\parallel}^L|^2) - 8 \frac{m_l}{\sqrt{q^2}} \text{Re}[\mathcal{A}_\perp^L \mathcal{A}_{T\perp}^{L*} + \mathcal{A}_\parallel^L \mathcal{A}_{T\parallel}^{L*}] \right] \\
I_{2c} &= -2N_F \left(1 - \frac{m_l^2}{q^2}\right) (|\mathcal{A}_0^L|^2 - |\mathcal{A}_{T0}^L|^2) \\
I_{2s} &= \frac{1}{2} N_F \left(1 - \frac{m_l^2}{q^2}\right) \left(|\mathcal{A}_\perp^L|^2 + |\mathcal{A}_\parallel^L|^2 - 4(|\mathcal{A}_{T\perp}^L|^2 + |\mathcal{A}_{T\parallel}^L|^2) \right) \\
I_3 &= N_F \left(1 - \frac{m_l^2}{q^2}\right) \left(|\mathcal{A}_\perp^L|^2 - |\mathcal{A}_\parallel^L|^2 - 4(|\mathcal{A}_{T\perp}^L|^2 + |\mathcal{A}_{T\parallel}^L|^2) \right) \\
I_4 &= \sqrt{2} N_F \left(1 - \frac{m_l^2}{q^2}\right) \text{Re}[\mathcal{A}_0 \mathcal{A}_\parallel^{L*} - 4\mathcal{A}_{T0}^L \mathcal{A}_{T\parallel}^{L*}] \\
I_5 &= 2\sqrt{2} N_F \left[\text{Re} \left[\left(\mathcal{A}_0^L - 2 \frac{m_l}{\sqrt{q^2}} \mathcal{A}_{T0}^L \right) \left(\mathcal{A}_\perp^{L*} - 2 \frac{m_l}{\sqrt{q^2}} \mathcal{A}_{T\perp}^{L*} \right) \right] - \frac{m_l^2}{q^2} \text{Re} \left[\mathcal{A}_{tP}^{L*} \left(\mathcal{A}_\parallel^L - 2 \frac{m_l}{\sqrt{q^2}} \mathcal{A}_{T\parallel}^L \right) \right] \right]
\end{aligned}$$

$$\begin{aligned}
I_{6c} &= N_F \frac{8m_l^2}{q^2} \text{Re}[\mathcal{A}_{tP}^{L*}(\mathcal{A}_0^L - 2\frac{\sqrt{q^2}}{m_l}\mathcal{A}_{T0}^L)] \\
I_{6s} &= 4N_F \text{Re}[(\mathcal{A}_{||}^L - 2\frac{m_l}{\sqrt{q^2}}\mathcal{A}_{T||}^L)(\mathcal{A}_{\perp}^{L*} - 2\frac{m_l}{\sqrt{q^2}}\mathcal{A}_{T\perp}^{L*})] \\
I_7 &= -2\sqrt{2}N_F \left[\text{Im}[(\mathcal{A}_0^L - 2\frac{m_l}{q^2}\mathcal{A}_{T0}^L)(\mathcal{A}_{||}^{L*} - 2\frac{m_l}{q^2}\mathcal{A}_{T||}^{L*}) + \frac{m_l^2}{q^2}\text{Im}[\mathcal{A}_{tP}^{L*}(\mathcal{A}_{\perp}^L - 2\frac{q^2}{m_l}\mathcal{A}_{T\perp}^L)]] \right] \\
I_8 &= \sqrt{2}N_F (1 - \frac{m_l^2}{q^2}) \text{Im}[\mathcal{A}_0^{L*}\mathcal{A}_{\perp}^L - 4\mathcal{A}_{T0}^{L*}\mathcal{A}_{T\perp}^L] \\
I_9 &= 2N_F (1 - \frac{m_l^2}{q^2}) \text{Im}[\mathcal{A}_{||}^L\mathcal{A}_{\perp}^{L*} - 4\mathcal{A}_{T||}^L\mathcal{A}_{T\perp}^{L*}], \tag{16}
\end{aligned}$$

with

$$N_F = \frac{G_F^2 |V_{cb}|^2}{2^7 3 \pi^3 m_{B_s}^3} q^2 \lambda_{D_s^*}^{1/2} (1 - \frac{m_l^2}{q^2})^2 \mathcal{B}(D_s^* \rightarrow D_s \pi). \tag{17}$$

The longitudinal, transverse and time like component of amplitude $\mathcal{A}_{T0, T\perp, T||}^L$, written in terms of NP couplings, are taken from Ref. [102]. We refer to Ref [102] for the omitted details.

1. The q^2 dependent observables

- The differential branching ratio, the lepton forward-backward asymmetry $A_{FB}^l(q^2)$, the forward-backward Asymmetry of transversely polarized D_s^* meson $A_{FB}^T(q^2)$ and the convexity parameter $C_F^l(q^2)$ can be defined as [60]

$$\begin{aligned}
\frac{d\Gamma}{dq^2}(q^2) &= \frac{1}{4} (6I_{1S} + 3I_{1c} - 2I_{2s} - I_{2c}), & A_{FB}^l(q^2) &= \frac{3}{8} \frac{(I_{6c} + 2I_{6s})}{d\Gamma/dq^2}, \\
A_{FB}^T(q^2) &= \frac{3}{8} \frac{I_{6s}}{d\Gamma_T/dq^2}, & C_F^l(q^2) &= \frac{6}{8} \frac{(2I_{2c} + 4I_{2s})}{d\Gamma/dq^2}. \tag{18}
\end{aligned}$$

- The angular observables $A_3(q^2)$, $A_4(q^2)$, $A_5(q^2)$, $A_{6s}(q^2)$, $A_7(q^2)$, $A_8(q^2)$ and $A_9(q^2)$ can be defined as [60]

$$\begin{aligned}
A_3(q^2) &= \frac{1}{2\pi} \frac{I_3}{d\Gamma/dq^2} & A_4(q^2) &= -\frac{2}{\pi} \frac{I_4}{d\Gamma/dq^2} \\
A_5(q^2) &= -\frac{3}{4} \frac{I_5}{d\Gamma/dq^2} & A_{6s}(q^2) &= -\frac{27}{8} \frac{I_{6s}}{d\Gamma/dq^2} \\
A_7(q^2) &= -\frac{3}{4} \frac{I_7}{d\Gamma/dq^2} & A_8(q^2) &= \frac{2}{\pi} \frac{I_8}{d\Gamma/dq^2} \\
A_9(q^2) &= \frac{1}{2\pi} \frac{I_9}{d\Gamma/dq^2}. \tag{19}
\end{aligned}$$

2. The $\cos\theta$ dependent observables

The $\cos\theta_{D_s}$ and $\cos\theta_l$ dependent observables can be defined as follows [63].

$$\begin{aligned}
F_L(\cos\theta_{D_s}) &= \frac{9}{16} \frac{\int_{q_{min}^2}^{q_{max}^2} (2I_{1c} - \frac{2}{3}I_{2c}) \cos^2\theta_{D_s} dq^2}{\Gamma(B_s \rightarrow D_s^* \rightarrow D_s^*(D\pi)l\nu)} \\
F_T(\cos\theta_{D_s}) &= \frac{9}{16} \frac{\int_{q_{min}^2}^{q_{max}^2} (2I_{1s} - \frac{2}{3}I_{2s})(1 - \cos^2\theta_{D_s}) dq^2}{\Gamma(B_s \rightarrow D_s^* \rightarrow D_s^*(D\pi)l\nu)} \\
F_L(\cos\theta_l) &= \frac{9}{24} \frac{\int_{q_{min}^2}^{q_{max}^2} (I_{1c} + I_{2c}(2\cos^2\theta_l - 1) + I_{6c}\cos\theta_l) dq^2}{\Gamma(B_s \rightarrow D_s^* \rightarrow D_s^*(D\pi)l\nu)}
\end{aligned}$$

$$\begin{aligned}
F_T(\cos \theta_l) &= \frac{9 \int_{q_{min}^2}^{q_{max}^2} (I_{1s} + I_{2s}(\cos^2 \theta_l - 1) + I_{6s} \cos \theta_l) dq^2}{12 \Gamma(B_s \rightarrow D_s^* \rightarrow D_s^*(D\pi)l\nu)} \\
A_{FB}^l(\cos \theta_{D_s}) &= \frac{9 \int_{q_{min}^2}^{q_{max}^2} (I_{6s} + (I_{6c} - I_{6s}) \cos^2 \theta_{D_s}) dq^2}{16 \frac{d\Gamma}{d \cos \theta_{D_s}}}, \tag{20}
\end{aligned}$$

where

$$\frac{d\Gamma}{d \cos \theta_{D_s}} = \frac{9}{24} \int_{q_{min}^2}^{q_{max}^2} [(3I_{1s} - I_{2s}) + (I_{2s} - 3I_{1s} + 3I_{1c} - 2I_{2c}) \cos^2 \theta_{D_s}] dq^2. \tag{21}$$

III. RESULTS AND DISCUSSION

A. Input Parameters

In Table I, we report all the theory inputs such as the masses of various mesons, leptons, the branching fraction of $\mathcal{B}(D_s^* \rightarrow D_s \gamma)$, $\mathcal{B}(D_s^* \rightarrow D_s \pi)$ and mass of b quark and c quark evaluated at renormalization scale $\mu = m_b$ [97]. The mass parameters are expressed in GeV unit and the B_s meson life time τ_{B_s} is expressed in second. We consider the uncertainties associated with the CKM matrix element $|V_{cb}|$ and the relevant vector and axial vector form factor inputs V , A_0 , A_1 and A_2 of Ref [98]. The relevant formula for the form factors pertinent for our discussion, taken from Ref. [98], is

$$F(q^2) = \frac{1}{P(q^2)} \sum_{n=0}^3 a_n z^n(q^2, t_0), \tag{22}$$

where F stands for the form factors V , A_0 , A_1 , A_2 and a_0 , a_1 , a_2 , a_3 are the z-expansion coefficients. The pole function $P(q^2)$ and $z(q^2, t_0)$ are defined as

$$P(q^2) = \prod_{M_{pole}} z(q^2, M_{pole}^2) \quad z(q^2, t_0) = \frac{\sqrt{t_+ - q^2} - \sqrt{t_+ - t_0}}{\sqrt{t_+ - q^2} + \sqrt{t_+ - t_0}}. \tag{23}$$

where, $t_0 = (M_{B_s} - M_{D_s^*})^2$, $t_+ = (M_B + M_{D^*})^2$ and the pole masses are represented by M_{pole} . In Table. II, we report the form factor inputs relevant for our analysis. The uncertainty associated with these parameters are written within parenthesis.

Parameters	Values	Parameters	Values	Parameters	Values
m_{B_s}	5.36677	$m_{D_s^*}$	2.112	m_e	$0.5109989461 \times 10^{-3}$
m_b	4.18	m_c	0.91	$ V_{cb} $	0.0409(11)
m_B	5.27964	m_{D^*}	2.010	m_τ	1.77682
$\mathcal{B}(D_s^* \rightarrow D_s \pi)$	5.8×10^{-2}	$\mathcal{B}(D_s^* \rightarrow D_s \gamma)$	93.5×10^{-2}		
G_F	1.1663787×10^{-5}	τ_{B_s}	1.515×10^{-12}		

TABLE I: Theory input parameters

	a_0	a_1	a_2	a_3	M_{pole}				
A_0	0.1046(79)	-0.39(15)	0.02(98)	-0.03(1.00)	6.275	6.872	7.25		
A_1	0.0536(28)	0.020(75)	0.09(81)	0.10(99)	6.745	6.75	7.15	7.15	
A_2	0.051(15)	0.02(26)	-0.35(79)	-0.07(99)	6.745	6.75	7.15	7.15	
V	0.102(14)	-0.27(30)	-0.007(0.998)	-3e-05 +- 1	6.335	6.926	7.02	7.28	

TABLE II: Form factor Input Parameters.

We have used the equation of motion to find out the relevant tensor form factors so that

$$\begin{aligned} T_1(q^2) &= \frac{m_b + m_c}{m_{B_s} + m_{D_s^*}} V(q^2), & T_2(q^2) &= \frac{m_b - m_c}{m_{B_s} - m_{D_s^*}} A_1(q^2), \\ T_3(q^2) &= -\frac{m_b - m_c}{q^2} \left[m_{B_s} (A_1(q^2) - A_2(q^2)) + m_{D_s^*} (A_2(q^2) + A_1(q^2) - 2A_0(q^2)) \right]. \end{aligned} \quad (24)$$

B. SM prediction

We report the SM central value and the 1σ uncertainty associated with several observables such as the branching ratio (BR), the ratio of branching ratio ($R_{D_s^*}$), the forward backward asymmetry (A_{FB}^l), the convexity parameter (C_F^l), the forward backward asymmetry for the transversely polarized D_s^* meson (A_{FB}^T), the longitudinal polarization fraction of D_s^* meson ($F_L^{D_s^*}$), A_3 , A_4 , A_5 , A_{6s} , A_7 , A_8 and A_9 for both e and τ mode in Table III. Our observations are as follows.

- The branching ratio of $B_s \rightarrow D_s^*(\rightarrow D_s\pi)l\nu$ mode is found to be of $\mathcal{O}(10^{-3})$, whereas the branching ratio of $B_s \rightarrow D_s^*(\rightarrow D_s\gamma)l\nu$ decay mode is obtained to be of $\mathcal{O}(10^{-2})$.
- As expected, the central value and the 1σ uncertainty associated with $R_{D_s^*}$, A_{FB}^l , C_F^l , A_{FB}^T and $F_L^{D_s^*}$ is exactly same for the $B_s \rightarrow D_s^*(\rightarrow D_s\gamma)l\nu$ and the $B_s \rightarrow D_s^*(\rightarrow D_s\pi)l\nu$ mode.
- The angular observables such as A_3 , A_4 , A_5 , A_{6s} are, however, quite different for both the decay modes. The central values obtained for A_3 , A_4 and A_5 in $B_s \rightarrow D_s^*(\rightarrow D_s\pi)l\nu$ mode are twice as large as the values obtained in case of $B_s \rightarrow D_s^*(\rightarrow D_s\gamma)l\nu$ mode.
- The angular observables A_7 , A_8 and A_9 are zero in the SM and are non-vanishing only if NP induces a complex contribution to the amplitude
- The ratio of branching ratio $R_{D_s^*}$ is found to be 0.2430 ± 0.0015 which is quite similar to the value reported in Ref [98].

Observable	$B_s \rightarrow D_s^*(\rightarrow D_s\pi)l\nu$ decay mode		$B_s \rightarrow D_s^*(\rightarrow D_s\gamma)l\nu$ decay mode	
	e -mode	τ mode	e mode	τ mode
	central value	Central value	central value	central value
BR	$(3.0516 \pm 0.0988) \times 10^{-3}$	$(0.7415 \pm 0.0231) \times 10^{-3}$	$(4.9194 \pm 0.1593) \times 10^{-2}$	$(1.1954 \pm 0.0372) \times 10^{-2}$
A_{FB}^l	-0.2640 ± 0.0031	-0.0896 ± 0.0020	-0.2640 ± 0.003	-0.0896 ± 0.0020
A_{FB}^T	-0.5436 ± 0.0035	-0.3842 ± 0.0026	-0.5436 ± 0.0035	-0.3842 ± 0.0026
$F_L^{D_s^*}$	0.5143 ± 0.0040	0.4482 ± 0.0015	0.5143 ± 0.0040	0.4482 ± 0.0015
A_3	-0.0252 ± 0.0003	-0.0162 ± 0.0001	0.0126 ± 0.0001	0.0081 ± 0.0001
A_4	0.1909 ± 0.0005	0.0883 ± 0.0001	-0.0954 ± 0.0002	-0.0442 ± 0.0001
A_5	-0.2139 ± 0.0019	-0.2265 ± 0.0010	0.1069 ± 0.0010	0.1133 ± 0.0005
A_{6s}	1.1882 ± 0.0140	0.9539 ± 0.0077	-0.0000 ± 0.0000	-0.5509 ± 0.0026
C_F^l	-0.4071 ± 0.0091	-0.0550 ± 0.0014	-0.4071 ± 0.0091	-0.0550 ± 0.0014
A_7	0.0000	0.0000	0.0000	0.0000
A_8	0.0000	0.0000	0.0000	0.0000
A_9	0.0000	0.0000	0.0000	0.0000
$R_{D_s^*}$	0.2430 ± 0.0015		0.2430 ± 0.0015	

TABLE III: The central values and the corresponding 1σ ranges of various observables in the SM.

In Fig1, we show several q^2 and $\cos\theta_l$ dependent observables such as $R_{D_s^*}(q^2)$, $A_{FB}^l(q^2)$, $A_{FB}^T(q^2)$, $F_L^{D_s^*}(q^2)$, $C_F^l(q^2)$, $F_L(\cos\theta_l)$ and $F_T(\cos\theta_l)$ for the $B_s \rightarrow D_s^*(\rightarrow D_s\gamma, D_s\pi)l\nu$ decay mode. It should be mentioned that these observables show exact same behaviour for the $D_s\pi$ and the $D_s\gamma$ mode. Here the red color represents the e mode and green color represents the τ mode, respectively. Our main observations are as follows.

- A_{FB}^l : We observe a zero crossing of A_{FB}^l at $q^2 = 5.25 \pm 0.12$ GeV².

- A_{FB}^T : A_{FB}^T is minimum at low q^2 and assumes negative values for the whole q^2 range in both e mode and τ mode. Moreover, it increases with q^2 and becomes zero at $q^2 = q_{\max}^2$.
- C_F^L : The convexity parameter $C_F^e(q^2)$ is found to be minimum at low q^2 and it increases as q^2 increases. At $q^2 = q_{\max}^2$, it is equal to zero for both e and the τ mode.
- $F_L^{D_s^*}$: The longitudinal polarization fraction $F_L^{D_s^*}$ is maximum for low value of q^2 . It gradually decreases and becomes minimum at $q^2 = q_{\max}^2$.
- $F_L^{D_s^*}(\cos\theta_l)$: The distribution is found to be symmetric in case of e mode but not for the τ mode. This is due to the presence of lepton mass term in the amplitude. At $\cos\theta_l = 0$, $F_L^{D_s^*}(\cos\theta_l)$ is maximum for e mode, whereas, for the τ mode, the maximum occurs at $\cos\theta_l = 1$.
- $F_T^{D_s^*}(\cos\theta_l)$: The maximum value of $F_T^{D_s^*}$ is obtained for $\cos\theta_l = -1$ for both e and the τ mode. It gradually decreases with increasing $\cos\theta_l$ and becomes minimum near $\cos\theta_l = 1$.

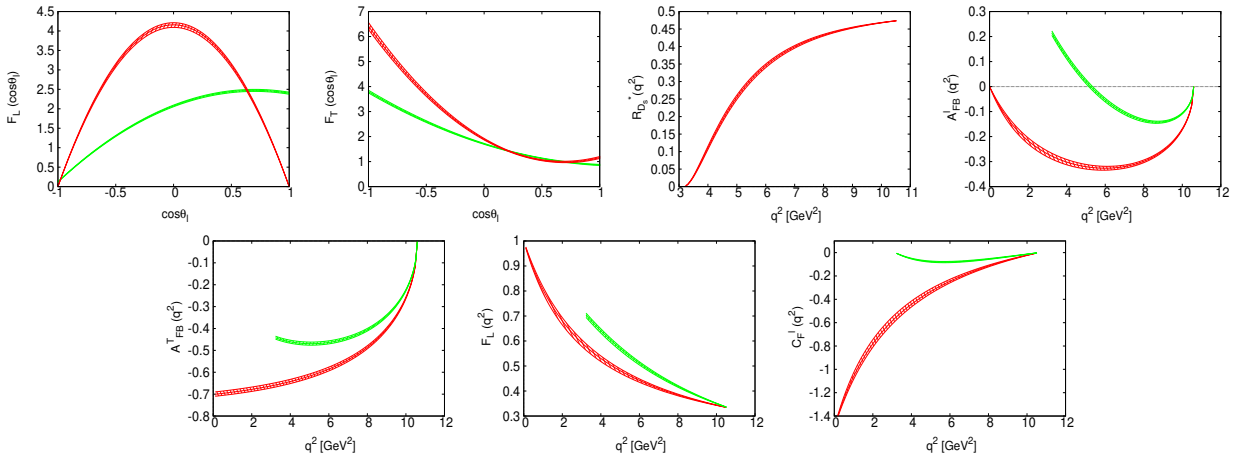


FIG. 1: q^2 and $\cos\theta_l$ dependence of $B_s \rightarrow D_s^*(\rightarrow D_s\gamma, D_s\pi)l\nu$ decay observables in the SM for the e (red) and the τ (green) mode.

In Fig 2, we display the q^2 and $\cos\theta_{D_s}$ dependence of several observables that are different for $B_s \rightarrow D_s^*(\rightarrow D_s\pi)l\nu$ and $B_s \rightarrow D_s^*(\rightarrow D_s\gamma)l\nu$ decay modes. Here the red color represents the e mode and green color represents the τ mode, respectively. Our observations are as follows.

- DBR : In case of $B_s \rightarrow D_s^*(\rightarrow D_s\gamma)l\nu$ decay mode, the maximum value of DBR = $(0.567 \pm 0.037) \times 10^{-2}$ is observed at $q^2 \approx 6.04 \text{ GeV}^2$ for the e mode, whereas, the maximum value of DBR = $(0.241 \pm 0.015) \times 10^{-2}$ is observed at $q^2 \approx 8.28 \text{ GeV}^2$ for the τ mode. Similarly, for $B_s \rightarrow D_s^*(\rightarrow D_s\pi)l\nu$, the DBR peak of $(0.351 \pm 0.023) \times 10^{-3}$ is observed at $q^2 \approx 6.15 \text{ GeV}^2$ for e mode and maximum DBR = $(0.150 \pm 0.010) \times 10^{-3}$ is observed at $q^2 \approx 8.07 \text{ GeV}^2$ for the τ mode.
- A_3, A_4, A_5 : The angular observables A_i s obey a strict relation $A_i^\tau = -2A_i^e$ at all values of q^2 for the $D_s\pi$ and $D_s\gamma$ mode.
- A_{6s} : For the $D_s\gamma$ channel, A_{6s} is observed to be zero for the e mode, whereas, it is minimum at low q^2 and maximum at high q^2 for the τ mode. It should also be mentioned that value of A_{6s} is negative for the whole q^2 range. For the $D_s\pi$ channel, the maximum of A_{6s} is observed at $q^2 \approx 5.98 \text{ GeV}^2$ for the e mode and it is observed at $q^2 \approx 7.28 \text{ GeV}^2$ for the τ mode.
- $F_L^{D_s^*}(\cos\theta_{D_s})$: The behaviour of $F_L^{D_s^*}$ is symmetric about $\cos\theta_{D_s}$. The maximum value of $F_L^{D_s^*}$ is obtained at $\cos\theta_{D_s} = 0$ for both e and the τ mode in the $D_s\gamma$ mode, whereas, in $D_s\pi$ mode, we observe a minimum at $\cos\theta_{D_s} = 0$.
- $F_T^{D_s^*}(\cos\theta_{D_s})$: $F_T^{D_s^*}$ is symmetric in $\cos\theta_{D_s}$ for both $D_s\gamma$ and $D_s\pi$ mode. $F_T^{D_s^*}$ is minimum at $\cos\theta_{D_s} = 0$, whereas, it is found to be maximum at $\cos\theta_{D_s} = \pm 1$ for the $D_s\gamma$ mode. For the $D_s\pi$ mode, the maximum, however, occurs at $\cos\theta_{D_s} = 0$ and it goes to zero at $\cos\theta_{D_s} = \pm 1$.

- $A_{FB}^l(\cos\theta_{D_s})$: A_{FB}^l is symmetric in $\cos\theta_{D_s}$ for both $D_s\gamma$ and $D_s\pi$ modes. For $D_s\gamma$ mode, A_{FB}^l is minimum at $\cos\theta = \pm 1$, whereas, it is maximum at $\cos\theta = 0$ for both e and the τ mode. However, for $D_s\pi$ mode, it is completely opposite. A_{FB}^l is maximum at $\cos\theta = \pm 1$ and minimum at $\cos\theta = 0$ for both e and the τ cases. It should also be mentioned that, a zero crossing in $A_{FB}^l(\cos\theta_{D_s})$ is observed at $\cos\theta_{D_s} = \pm 0.456 \pm 0.018$ for the $D_s\gamma$ mode, whereas, the zero crossing point is observed at $\cos\theta_{D_s} = \pm 0.626 \pm 0.007$ for the $D_s\pi$ mode.

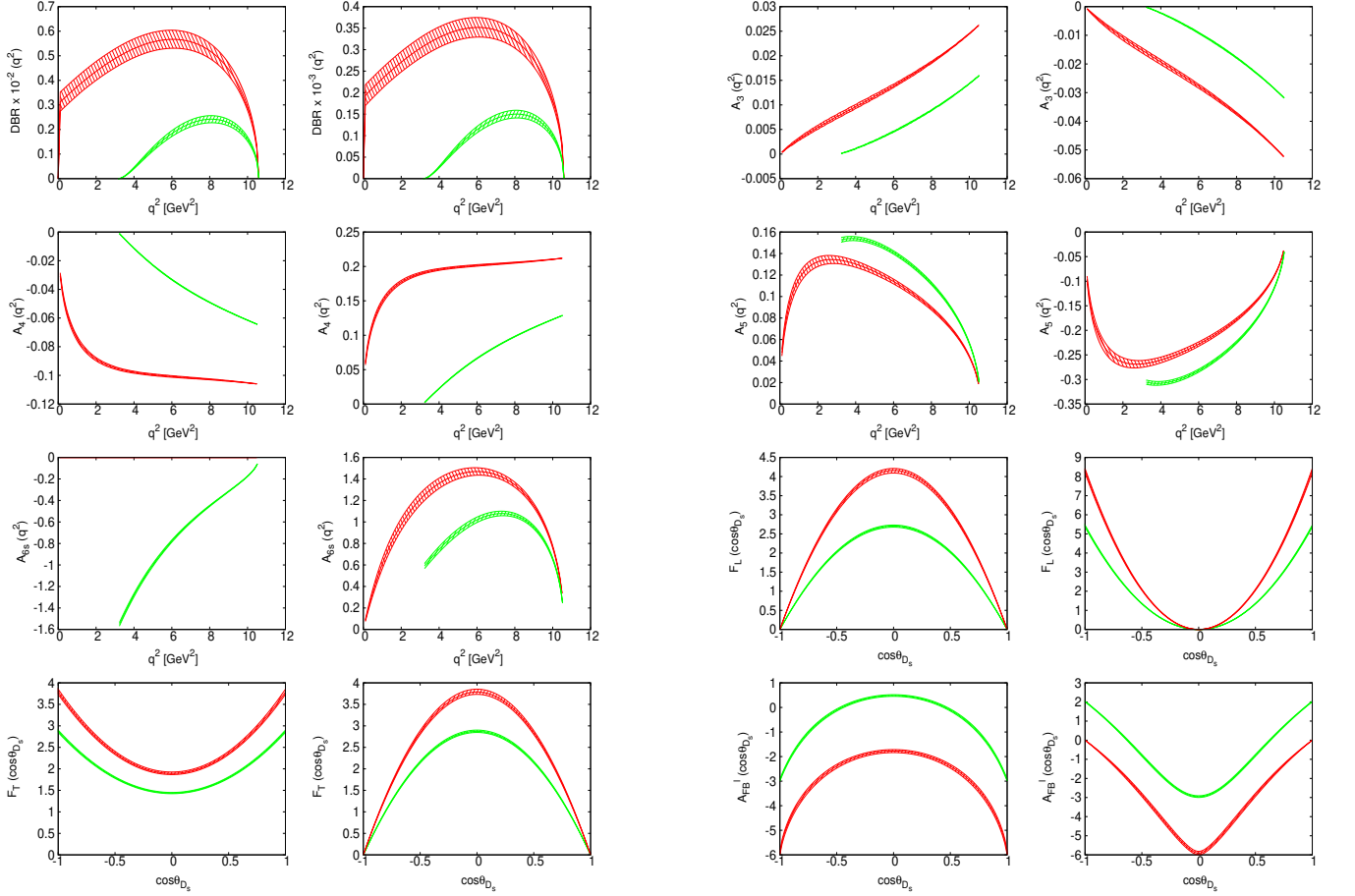


FIG. 2: q^2 and $\cos\theta_{D_s}$ dependence of $B_s \rightarrow D_s^*(\rightarrow D_s\gamma, D_s\pi) l\nu$ decay observables in the SM for the e (red) and the τ (green) mode.

C. New physics analysis

We now proceed to discuss the NP effects on various physical observables in the angular distribution of $B_s \rightarrow D_s^*(\rightarrow D_s\gamma)\tau\nu$ and $B_s \rightarrow D_s^*(\rightarrow D_s\pi)\tau\nu$ decays in a model independent framework. We have taken three possible NP scenarios. The best fit values of the NP couplings under each scenarios, taken from recent global fit analysis [60, 78, 79], are reported in Table IV.

1. Scenario - I

In scenario - I, we choose four different 1D NP hypothesis and the corresponding best fit values of Ref [78, 79] obtained at scale $\mu = 1\text{TeV}$ are reported in Table IV. For our analysis, we run these NP couplings down to the renormalization scale $\mu = m_b$ [78, 79]. The effect of these NP couplings on several physical observables pertaining to $B_s \rightarrow D_s^*(\rightarrow D_s\gamma)\tau\nu$ and $B_s \rightarrow D_s^*(\rightarrow D_s\pi)\tau\nu$ decay modes are reported in Table V.

New physics scenarios		
Scenerio - I [78, 79]	Scenerio - II [78, 79]	Scenerio - III [60]
$g_{V_L} = 0.07$	$(g_{V_L}, g_{S_L} = -4g_{T_L}) = (0.10, -0.04)$	$g_{V_L} = 0.07 - i0.16$
$g_{S_R} = 0.09$	$(g_{S_R}, g_{S_L}) = (0.21, -0.15)(SetA)$ or	$g_{V_R} = -0.01 - i0.39$
$g_{S_L} = 0.07$	$(g_{S_R}, g_{S_L}) = (-0.26, -0.61)(SetB)$	$g_{S_L} = 0.29 - i0.67$
$g_{S_L} = 4g_{T_L} = -0.03$	$(g_{V_L}, g_{S_R}) = (0.08, -0.01)$	$g_{S_R} = 0.19 + i0.08$
	$(g_{S_L} = 4g_{T_L}) = (-0.06 + i0.31)$	$g_{T_L} = 0.11 - i0.18$

TABLE IV: Best fit value of NP couplings.

It is clear from from Table V that in the presence of g_{V_L} NP coupling, the branching ratio gets considerable deviations from the SM predication. However, no deviation from the SM prediction is observed for observables that are in the form of ratios. The NP dependency cancels in these ratios. In the presence of g_{S_L} and g_{S_R} NP couplings, A_{FB}^τ is found to be at more than 4σ away from the SM prediction for both $D_s\gamma$ and $D_s\pi$ mode. Similarly, a deviation of around 3.4σ , 4.71σ and 1σ is observed for $F_L^{D_s^*}$ in the presence of g_{S_L} , g_{S_R} and $g_{S_L} = 4g_{T_L}$ NP couplings. Moreover, the deviation from the SM expectation observed in case of $R_{D_s^*}$ is at the level of 2.05σ and 3.96 significance in the presence of g_{S_R} and $g_{S_L} = 4g_{T_L}$ NP couplings respectively, whereas, it is at the level of 15σ significance for g_{V_L} NP coupling. The observables A_3 and A_{FB}^T show slight deviation from the SM in the presence of $g_{S_L} = 4g_{T_L}$ NP coupling. As expected, A_7 , A_8 and A_9 are all zero and hence we don't report them in Table. V.

	g_{V_L}		g_{S_L}		g_{S_R}		$g_{S_L} = 4g_{T_L}$	
	$D_s\gamma$	$D_s\pi$	$D_s\gamma$	$D_s\pi$	$D_s\gamma$	$D_s\pi$	$D_s\gamma$	$D_s\pi$
$BR \times 10^{-2}$	1.3686 ± 0.0426	0.0849 ± 0.0026	1.1798 ± 0.0367	0.0732 ± 0.0023	1.2174 ± 0.0379	0.0755 ± 0.0024	1.2382 ± 0.0385	0.0768 ± 0.0024
A_3	0.0081 ± 0.0001	-0.0162 ± 0.0001	0.0082 ± 0.0001	-0.0164 ± 0.0001	0.0080 ± 0.0001	-0.0159 ± 0.0001	0.0078 ± 0.0001	-0.0156 ± 0.0001
A_4	-0.0442 ± 0.0001	0.0883 ± 0.0001	-0.0448 ± 0.0001	0.0895 ± 0.0001	-0.0434 ± 0.0001	0.0867 ± 0.0001	-0.0426 ± 0.0001	0.0852 ± 0.0001
A_5	0.1133 ± 0.0005	-0.2265 ± 0.0010	0.1104 ± 0.0005	-0.2208 ± 0.0010	0.1166 ± 0.0005	-0.2333 ± 0.0010	0.1119 ± 0.0005	-0.2238 ± 0.0010
A_{6s}	-0.5509 ± 0.0026	0.9539 ± 0.0077	-0.5076 ± 0.0025	0.9665 ± 0.0078	-0.6033 ± 0.0028	0.9366 ± 0.0076	-0.5673 ± 0.0027	0.9098 ± 0.0075
$R_{D_s^*}$	0.2782 ± 0.0018		0.2398 ± 0.0015		0.2475 ± 0.0016		0.2517 ± 0.0016	
A_{FB}^τ	-0.0896 ± 0.0020		-0.1020 ± 0.0020		-0.0741 ± 0.0021		-0.0761 ± 0.0020	
A_{FB}^T	-0.3842 ± 0.0026		-0.3842 ± 0.0026		-0.3842 ± 0.0026		-0.3677 ± 0.0025	
F_L	0.4482 ± 0.0015		0.4409 ± 0.0015		0.4582 ± 0.0015		0.4501 ± 0.0015	
C_F^T	-0.0550 ± 0.0014		-0.0557 ± 0.0014		-0.0540 ± 0.0014		-0.0531 ± 0.0013	

TABLE V: Prediction of $B_s \rightarrow D_s^*(\rightarrow D_s\gamma, D_s\pi) \tau \nu$ decay observables in Scenerio - I.

In Fig 3 we display the q^2 and $\cos\theta_l$ dependence of several physical observables that exhibit same behaviour for the $D_s\gamma$ and $D_s\pi$ modes. The contribution coming from g_{V_L} , g_{S_L} , g_{S_R} , $g_{S_L} = 4g_{T_L}$ NP couplings are represented by blue, black, violet and orange lines, respectively. Our observations are as follows.

- In case of $F_L(\cos\theta_l)$, a slight deviation from SM expectation is observed at $\cos\theta_l \geq 0.5$ with g_{S_L} and g_{S_R} NP couplings and they are distinguishable from the SM prediction at slightly more than 1σ significance. However, for $F_T(\cos\theta_l)$, no such deviation is observed and they all lie within the SM error band.
- In case of $R_{D_s^*}(q^2)$, maximum deviation is observed in case of g_{V_L} NP coupling and it is clearly distinguishable from the SM prediction at more than 3σ significance at high q^2 value.
- The zero crossing in $A_{FB}^\tau(q^2)$ is shifted to lower value of q^2 than in the SM with g_{S_L} NP coupling, whereas, it is found to be shifted to higher value of q^2 with g_{S_R} and $g_{S_L} = 4g_{T_L}$ NP couplings. The zero crossings in A_{FB}^τ at $q^2 = 5.06 \text{ GeV}^2$, $q^2 = 5.48 \text{ GeV}^2$ and $q^2 = 5.43 \text{ GeV}^2$ in the presence of g_{S_L} , g_{S_R} and $g_{S_L} = 4g_{T_L}$ NP couplings are clearly distinguishable from the SM prediction of $q^2 = 5.25 \pm 0.12 \text{ GeV}^2$ at the level of 1.9σ and 2.3σ and 1.7σ significance.
- At low q^2 range, $A_{FB}^T(q^2)$ is deviates from the SM predication in the presence of $g_{S_L} = 4g_{T_L}$ NP coupling. In case of $F_L^{D_s^*}(q^2)$ and $C_F^T(q^2)$ observables, no significant deviation is observed and they all lie within the SM error band.

In Fig 4 we display the q^2 and $\cos\theta_{D_s}$ dependence of several physical observables that exhibits different behaviour for the $D_s\gamma$ and $D_s\pi$ decay modes. Our observations are as follows.

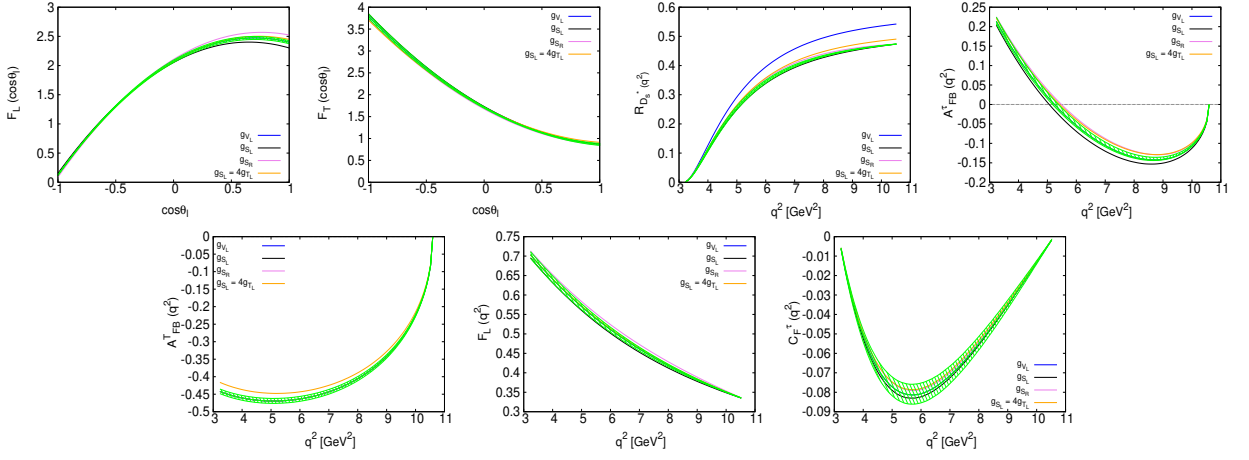


FIG. 3: The q^2 and $\cos \theta_l$ dependence of $B_s \rightarrow D_s^*(\rightarrow D_s \gamma, D_s \pi) \tau \nu$ decay observables in the SM and in the presence of the NP couplings of scenario - I. The SM central line and the corresponding error band are shown with green color. The blue, black, violet and orange lines represent the effect of g_{V_L} , g_{S_L} , g_{S_R} , $g_{S_L} = 4g_{T_L}$ NP couplings, respectively.

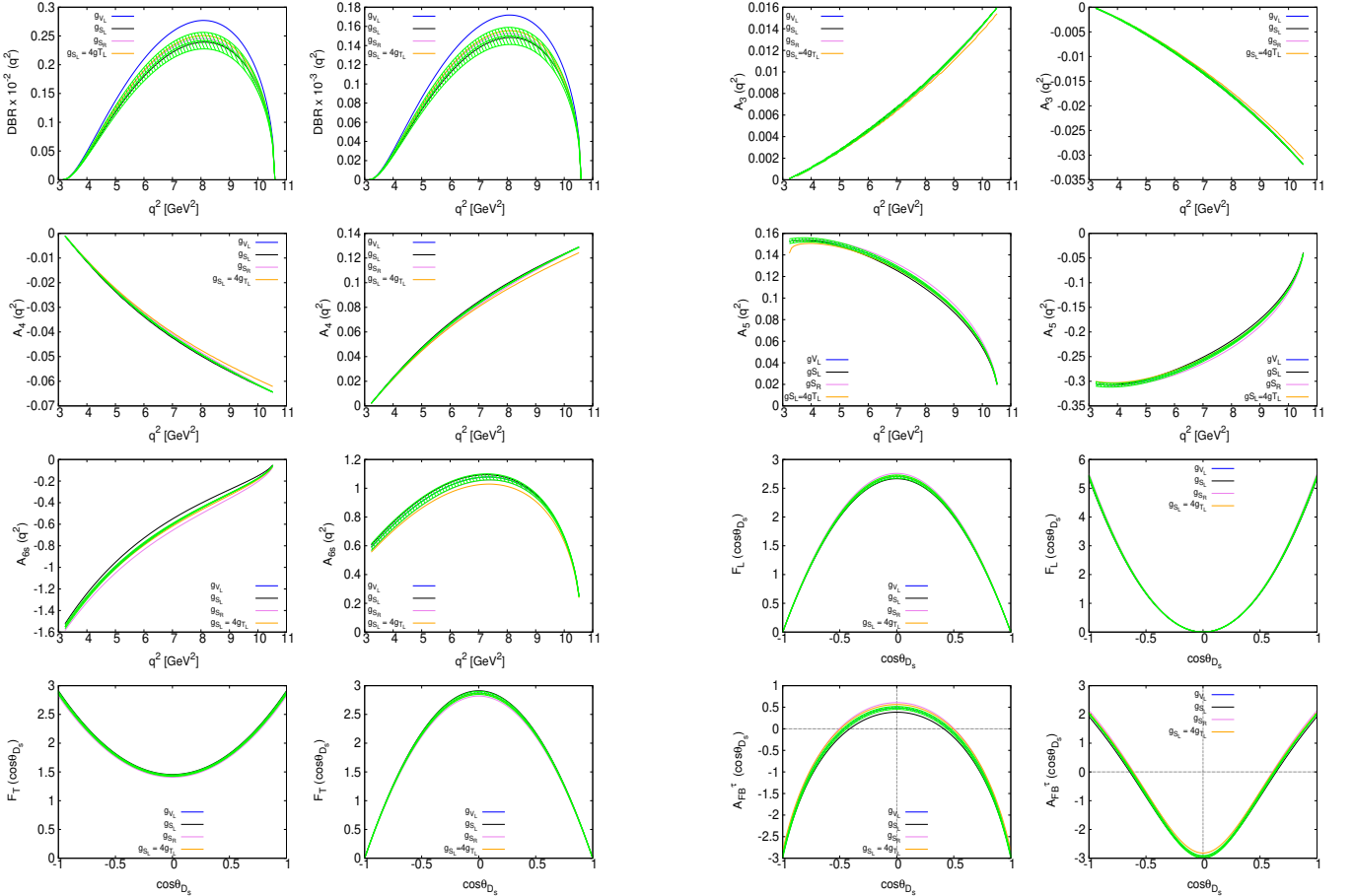


FIG. 4: The q^2 and $\cos \theta_{D_s}$ dependence of various physical observable of $B_s \rightarrow D_s^*(\rightarrow D_s \gamma, D_s \pi) \tau \nu$ in the SM and in the presence of the NP couplings of scenario - I. The SM central line and the corresponding error band are shown with green color. The blue, black, violet and orange colors represents the effect of NP coupling g_{V_L} , g_{S_L} , g_{S_R} , $g_{S_L} = 4g_{T_L}$ respectively.

- In case of differential branching ratio $DBR(q^2)$, the deviation from the SM prediction is more pronounced with g_{V_L} NP coupling and the peak of the distribution is clearly distinguishable from the SM prediction at the level of 2σ significance. No such significant deviation is observed with the rest of the NP couplings and they all lie within the SM error band.
- The angular observable A_3 , A_4 and A_5 are slightly deviated from the SM in the presence of $g_{S_L} = 4g_{T_L}$ NP coupling. Similarly in case of A_{6s} , a slight deviation is observed with g_{S_L} , g_{S_R} and $g_{S_L} = 4g_{T_L}$ NP coupling for the $D_s\gamma$ mode, whereas, A_{6s} shows slight deviation in the presence of $g_{S_L} = 4g_{T_L}$ for the $D_s\pi$ mode.
- The observables $F_L(\cos\theta_{D_s})$ and $F_T(\cos\theta_{D_s})$ do not show any significant deviation from the SM prediction in the presence of the NP couplings of scenario - I.
- The deviation from the SM prediction observed in case of $A_{FB}^{\tau}(\cos\theta_{D_s})$ is more pronounced with g_{S_L} , g_{S_R} and $g_{S_L} = 4g_{T_L}$ NP couplings for the $D_s\gamma$ mode. The zero crossing in $A_{FB}^{\tau}(\cos\theta_{D_s})$ is shifted to $\cos\theta_{D_s} = 0.412$, 0.500 and 0.497 in the presence of g_{S_L} , g_{S_R} and $g_{S_L} = 4g_{T_L}$ NP couplings and they are clearly distinguishable from the SM zero crossing of $\cos\theta_{D_s} = \pm 0.456 \pm 0.018$ at the level of more than 2σ significance. Similarly for the $D_s\pi$ mode, $A_{FB}^{\tau}(\cos\theta_{D_s})$ shows slight deviation in the presence of g_{S_L} , g_{S_R} and $g_{S_L} = 4g_{T_L}$ NP couplings. The zero crossings in $A_{FB}^{\tau}(\cos\theta_{D_s})$ observed at $\cos\theta_{D_s} = \pm 0.642$, ± 0.610 and ± 0.613 in the presence of g_{S_L} , g_{S_R} and $g_{S_L} = 4g_{T_L}$ NP couplings are distinguishable from the SM zero crossing of $\cos\theta_{D_s} = \pm 0.626 \pm 0.007$ at the level of $1 - 2\sigma$ significance.

2. (Scenario - II)

In scenerio-II, we choose four 2D NP hypothesis such as $(g_{V_L}, g_{S_L} = -4g_{T_L})$, (g_{S_R}, g_{S_L}) (Set A or Set B), (g_{V_L}, g_{S_R}) and $(g_{S_L} = 4g_{T_L})$. The best fit values of these NP couplings at $\mu = 1\text{TeV}$ scale obtained from Ref. [78, 79] are mentioned in the Table IV. In our analysis, we run them down to the renormalization scale of $\mu = m_b$. In Table VI, we report the central values and the corresponding 1σ range of several physical observables for both $B_s \rightarrow (D_s\gamma)\tau\nu$ and $B_s \rightarrow (D_s\pi)\tau\nu$ decays in the presence of each 2D NP couplings.

The deviation from the SM prediction observed for BR is more pronounced in the presence of $(g_{V_L}, g_{S_L} = -4g_{T_L})$ NP coupling and it is clearly distinguishable from the SM prediction at more than 3σ significance. Similarly, a deviation of around $2 - 3\sigma$ is observed with (g_{S_R}, g_{S_L}) (setA or Set B) and (g_{V_L}, g_{S_R}) NP couplings. Significant deviation from the SM prediction is observed for $R_{D_s^*}$ with $(g_{V_L}, g_{S_L} = -4g_{T_L})$, (g_{V_L}, g_{S_R}) and (g_{S_R}, g_{S_L}) (set A or Set B) NP couplings. In case of $F_L^{D_s^*}$, the deviation is more pronounced with (g_{S_R}, g_{S_L}) (set A or Set B) NP couplings. The angular observable A_7 is found to be non zero in the presence of $(g_{S_L} = 4g_{T_L})$ complex NP couplings for both $D_s\gamma$ and $D_s\pi$ modes. The angular observables A_8 and A_9 are absent in this scenario-II and hence we do not report them in Table- VI.

	$(g_{V_L}, g_{S_L} = -4g_{T_L})$		(g_{S_R}, g_{S_L}) (Set A)		(g_{S_R}, g_{S_L}) (Set B)		(g_{V_L}, g_{S_R})		$g_{S_L} = 4g_{T_L}$	
	$D_s\gamma$	$D_s\pi$	$D_s\gamma$	$D_s\pi$	$D_s\gamma$	$D_s\pi$	$D_s\gamma$	$D_s\pi$	$D_s\gamma$	$D_s\pi$
$BR \times 10^{-2}$	1.4049 ± 0.0437	0.0872 ± 0.0027	1.2984 ± 0.0404	0.0805 ± 0.0025	1.2963 ± 0.0404	0.0804 ± 0.0025	1.3918 ± 0.0433	0.0863 ± 0.0027	1.3696 ± 0.0426	0.0850 ± 0.0026
A_3	0.0083 ± 0.0001	-0.0167 ± 0.0001	0.0075 ± 0.0001	-0.0149 ± 0.0001	0.0075 ± 0.0001	-0.0150 ± 0.0001	0.0081 ± 0.0001	-0.0162 ± 0.0001	0.0066 ± 0.0001	-0.0132 ± 0.0001
A_4	-0.0454 ± 0.0001	0.0909 ± 0.0002	-0.0407 ± 0.0001	0.0813 ± 0.0002	-0.0407 ± 0.0001	0.0815 ± 0.0002	-0.0443 ± 0.0001	0.0885 ± 0.0001	-0.0359 ± 0.0001	0.0719 ± 0.0001
A_5	0.1178 ± 0.0005	-0.2356 ± 0.0010	0.1247 ± 0.0004	-0.2493 ± 0.0009	0.1245 ± 0.0004	-0.2490 ± 0.0009	0.1129 ± 0.0005	-0.2258 ± 0.0010	0.1084 ± 0.0004	-0.2168 ± 0.0008
A_{6s}	-0.5736 ± 0.0028	0.9950 ± 0.0079	-0.7422 ± 0.0030	0.8782 ± 0.0072	-0.7394 ± 0.0030	0.8796 ± 0.0072	-0.5453 ± 0.0026	0.9556 ± 0.0078	-0.6032 ± 0.0027	0.7508 ± 0.0061
A_7	0.0000	0.0000	0.0000	0.0000	0.0000	0.0000	0.0000	0.0000	0.0086 ± 0.0001	0.0172 ± 0.0001
$R_{D_s^*}$	0.2856 ± 0.0018		0.2639 ± 0.0018		0.2635 ± 0.0018		0.2829 ± 0.0018		0.2784 ± 0.0018	
A_{FB}^{τ}	-0.0936 ± 0.0021		-0.0302 ± 0.0021		-0.0311 ± 0.0021		-0.0912 ± 0.0020		-0.0328 ± 0.0017	
A_{FB}^{π}	-0.4047 ± 0.0026		-0.3842 ± 0.0026		-0.3842 ± 0.0026		-0.3842 ± 0.0026		-0.3000 ± 0.0017	
F_L	0.4537 ± 0.0015		0.4920 ± 0.0015		0.4912 ± 0.0015		0.4472 ± 0.0015		0.4438 ± 0.0015	
C_F	-0.0567 ± 0.0014		-0.0506 ± 0.0013		-0.0507 ± 0.0013		-0.0551 ± 0.0014		-0.0559 ± 0.0011	

TABLE VI: Prediction of $B_s \rightarrow D_s^*(\rightarrow D_s\gamma, D_s\pi)\tau\nu$ decay observables in Scenerio - II.

We display the q^2 and $\cos\theta_l$ dependence of several physical observables that show same behaviour for the $D_s\gamma$ and $D_s\pi$ decay modes in Fig 5. The blue, black, yellow, violet and red lines represent the contribution coming from $(g_{V_L}, g_{S_L} = -4g_{T_L})$, (g_{S_R}, g_{S_L}) (Set A), (g_{S_R}, g_{S_L}) (Set B), (g_{V_L}, g_{S_R}) and $(g_{S_L} = 4g_{T_L})$ NP couplings, respectively. Our observations are as follows.

- Although a slight deviation from the SM prediction is observed for $F_L(\cos\theta_l)$ with $g_{S_L} = 4g_{T_L}$ NP coupling, the deviation, however, is quite significant in the presence of (g_{S_R}, g_{S_L}) (Set A or Set B) NP couplings. Similarly, $F_T(\cos\theta_l)$ is observed to be deviated from the corresponding SM value in the presence of (g_{S_R}, g_{S_L}) (Set A or Set B) and $(g_{S_L} = 4g_{T_L})$ NP couplings.

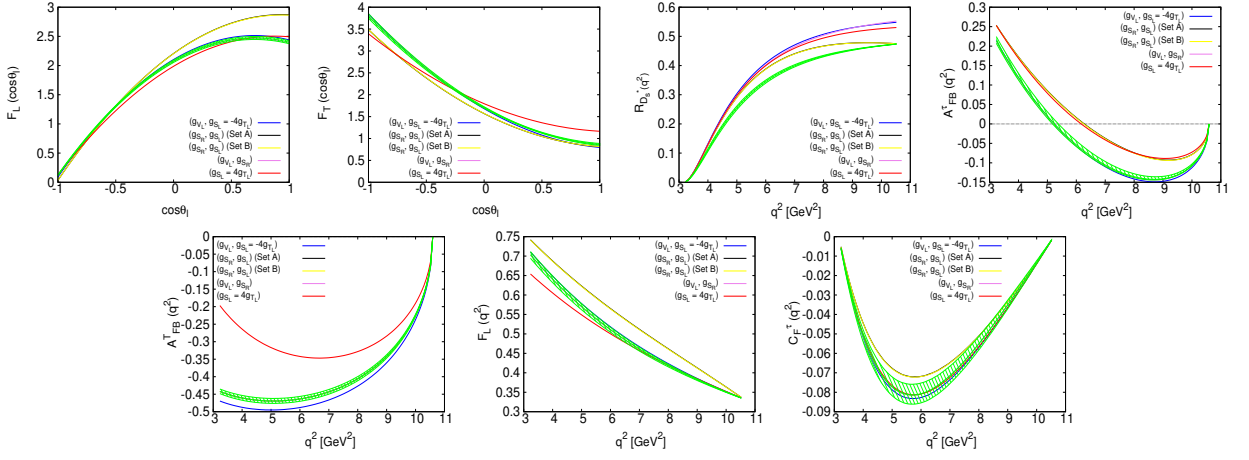


FIG. 5: The q^2 and $\cos \theta_l$ dependence of various physical observable of $B_s \rightarrow D_s^* (\rightarrow D_s \gamma, D_s \pi) \tau \nu$ in the SM and in the presence of the NP couplings of scenario - II. The SM central line and the corresponding error band are shown with green color. The blue, black, yellow, violet and red color represents the effect of NP coupling $(g_{V_L}, g_{S_L} = -4g_{T_L})$, (g_{S_R}, g_{S_L}) (Set A), (g_{S_R}, g_{S_L}) (Set B), (g_{V_L}, g_{S_R}) and $g_{S_L} = 4g_{T_L}$ respectively.

- Although the deviation from the SM prediction for $R_{D_s^*}(q^2)$ is quite significant for all the 2D NP couplings, it is more pronounced in case of $(g_{V_L}, g_{S_L} = -4g_{T_L})$, (g_{V_L}, g_{S_R}) and $(g_{S_L} = 4g_{T_L})$ NP couplings and they are clearly distinguishable from the SM prediction at more than 10σ significance.
- The zero crossing in $A_{FB}^{\tau}(q^2)$ is shifted to higher value of q^2 than in the SM in the presence of (g_{S_R}, g_{S_L}) (Set A or Set B) and $(g_{S_L} = 4g_{T_L})$ NP couplings. The zero crossings of $A_{FB}^{\tau}(q^2)$ at $q^2 = 6.28\text{GeV}^2$ and $q^2 = 6.16\text{GeV}^2$ in the presence of these NP couplings are clearly distinguishable from the SM prediction of $q^2 = 5.25 \pm 0.10\text{GeV}^2$ at more than 8σ significance. Similarly, for $A_{FB}^{\tau}(q^2)$, a significant deviation of more than 10σ is observed at low q^2 in the presence of $g_{S_L} = 4g_{T_L}$ NP coupling.
- In case of $F_L(q^2)$, although a slight deviation is observed with $(g_{S_L} = 4g_{T_L})$ NP coupling, the deviation, however, is more pronounced in the presence of (g_{S_R}, g_{S_L}) (Set A or Set B) NP couplings. Similarly for $C_F^{\tau}(q^2)$, maximum deviation from the SM prediction is observed with (g_{S_R}, g_{S_L}) (Set A or Set B) NP couplings.

The q^2 and $\cos \theta_{D_s}$ dependent observables which exhibit different behaviour for $D_s \pi$ and $D_s \gamma$ modes are displayed in Fig 6. The left panel figures correspond to the $D_s \gamma$ mode and right panel figures correspond to the $D_s \pi$ mode, respectively. Our observations are as follows.

- In case of $DBR(q^2)$, although there is deviation from the SM prediction with all NP couplings, the deviation, however, is more pronounced once the $(g_{V_L}, g_{S_L} = -4g_{T_L})$ NP coupling is switched on and it is clearly distinguishable from the SM prediction at more than 3σ significance level.
- For the A_3, A_4 and A_5 observables, the maximum deviation is observed in case of $(g_{S_L} = 4g_{T_L})$ NP couplings for both $D_s \pi$ and $D_s \gamma$ modes. For A_{6s} , the maximum deviation is observed with (g_{S_R}, g_{S_L}) (Set A or Set B) for the $D_s \gamma$ mode, whereas, for the $D_s \pi$ mode, the maximum deviation is observed with $(g_{S_L} = 4g_{T_L})$ NP coupling.
- For the $D_s \gamma$ mode, $F_L(\cos \theta_{D_s})$ deviates significantly from the SM prediction at $\cos \theta_{D_s} = 0$ in presence of (g_{S_R}, g_{S_L}) (Set A or Set B) NP coupling and it is clearly distinguishable from the SM error band, whereas, for the $D_s \pi$ mode, $F_L(\cos \theta_{D_s})$ shows a significant deviation at $\cos \theta_{D_s} = \pm 1$. In case of $F_T(\cos \theta_{D_s})$, the deviation from the SM prediction is more pronounced with (g_{S_R}, g_{S_L}) (Set A or Set B) NP couplings for both $D_s \pi$ and $D_s \gamma$ modes.
- For $D_s \gamma$ and $D_s \pi$ mode, $A_{FB}^{\tau}(\cos \theta_{D_s})$ deviates significantly from the SM prediction in the presence of (g_{S_R}, g_{S_L}) (Set A or Set B) and $(g_{S_L} = 4g_{T_L})$ NP couplings. The zero crossings in $A_{FB}^{\tau}(\cos \theta_{D_s})$ at $\cos \theta_{D_s} = \pm 0.601$ and $\cos \theta_{D_s} = \pm 0.563$ for $D_s \gamma$ and $D_s \pi$ modes lie 8σ away from the SM zero crossing point.
- We observe a non-zero q^2 distribution of $A_7(q^2)$ in the presence of $g_{S_L} = 4g_{T_L}$ complex NP couplings.

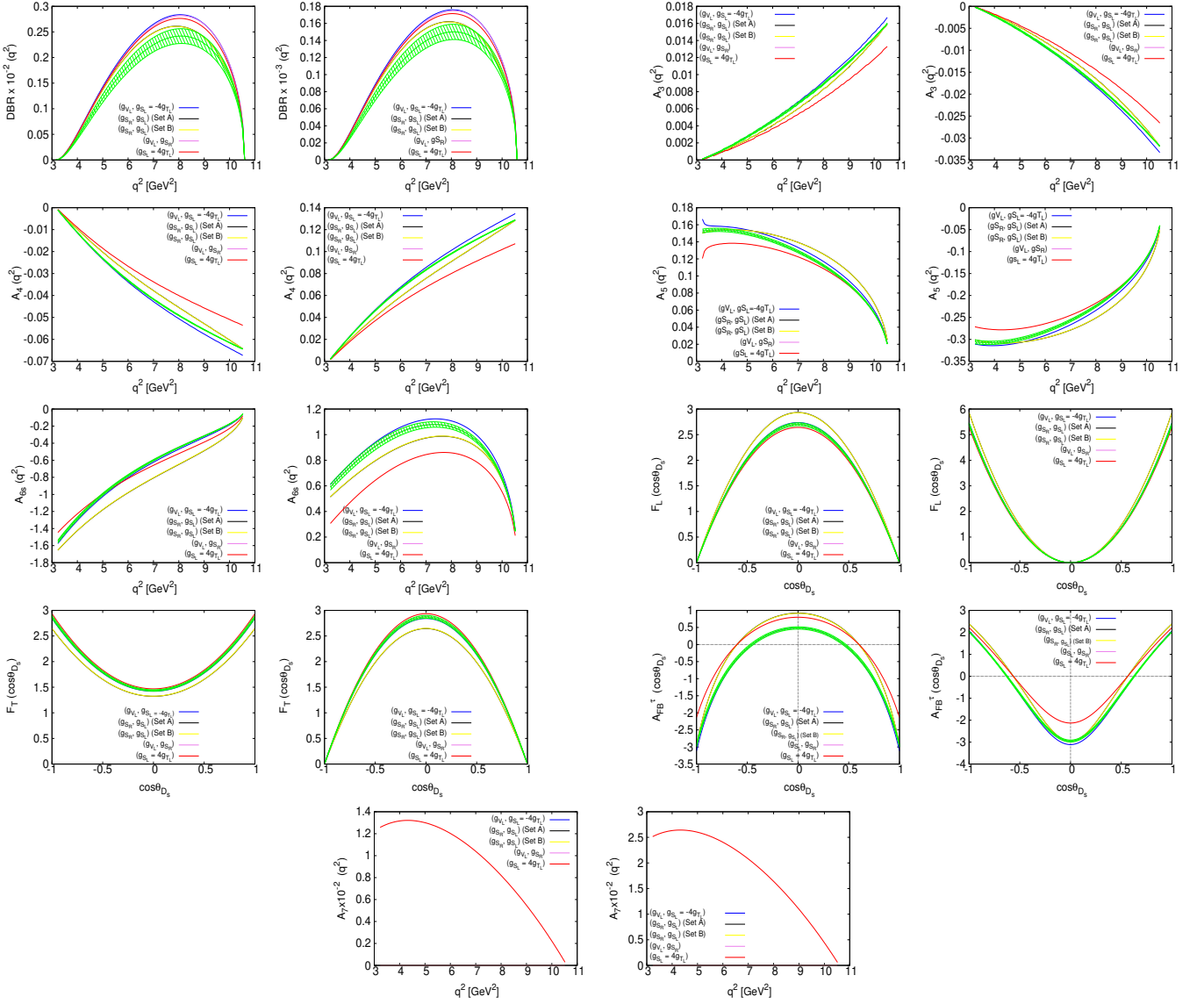


FIG. 6: The q^2 and $\cos\theta_{D_s}$ dependence of various physical observable of $B_s \rightarrow D_s^*(\rightarrow D_s\gamma, D_s\pi)\tau\nu$ in the SM and in the presence of the NP couplings of scenario - II. The SM central line and the corresponding error band are shown with green color. The blue, black, yellow, violet and red color colors represents the effect of NP coupling $(g_{V_L}, g_{S_L} = -4g_{T_L})$, (g_{S_R}, g_{S_L}) (Set A), (g_{S_R}, g_{S_L}) (Set B), (g_{V_L}, g_{S_R}) and $g_{S_L} = 4g_{T_L}$ respectively.

3. (Scenario - III)

In this scenario, we select five different complex 1D NP couplings. The best fit values each NP couplings at renormalization scale $\mu = m_b$ obtained from Ref[60] are reported in Table IV. In Table VII, we report the impact of each NP couplings on various physical observable in $D_s\gamma$ and $D_s\pi$ decay modes. We see significant deviation of all the observables with these complex NP couplings. In the presence of g_{V_L} and g_{V_R} NP couplings, branching ratio deviates from the SM prediction at the level of 3 – 6 σ significance. A_{FB}^T deviates more than 9 σ in the presence of g_{V_R} and g_{S_L} NP couplings and the observable A_{FB}^T deviates more than 10 σ from the SM expectation in case of g_{V_R} NP coupling. Similarly, the longitudinal polarization fraction of D_s^* , F_L is found to deviate from the SM value at more than 10 σ significance in the presence of g_{T_L} NP coupling for both the decay modes. In case of $R_{D_s^*}$, we observe a considerable deviation of around 10 σ in the presence of g_{V_L} and g_{T_L} NP couplings. Moreover, for A_3 , A_4 , and A_5 the maximum deviation from the SM prediction is observed with g_{T_L} NP coupling. For the angular observable A_{6s} , the deviation observed is more pronounced in case of g_{S_L} , g_{S_R} and g_{T_L} NP couplings in $D_s\gamma$ mode, whereas, g_{V_L} and g_{T_L} show more significant deviation in case of $D_s\pi$ mode. A nonzero value of A_7 is also observed in the presence of

g_{S_L} , g_{S_R} and g_{T_L} NP couplings. The angular observables A_8 and A_9 assume non zero values once g_{V_R} NP coupling is switched on. It should also be mentioned that the values of A_7 , A_8 and A_9 in $D_s\pi$ mode is twice as large as the values obtained for the $D_s\gamma$ mode.

	g_{V_L}		g_{V_R}		g_{S_L}		g_{S_R}		g_{T_L}	
	$D_s\gamma$	$D_s\pi$	$D_s\gamma$	$D_s\pi$	$D_s\gamma$	$D_s\pi$	$D_s\gamma$	$D_s\pi$	$D_s\gamma$	$D_s\pi$
$BR \times 10^{-2}$	1.3992 ± 0.0436	0.0868 ± 0.0027	1.3980 ± 0.0435	0.0867 ± 0.0027	1.1831 ± 0.0368	0.0734 ± 0.0023	1.2228 ± 0.0381	0.0759 ± 0.0024	1.3681 ± 0.0429	0.0849 ± 0.0027
A_3	0.0081 ± 0.0001	-0.0162 ± 0.0001	0.0082 ± 0.0001	-0.0163 ± 0.0001	0.0082 ± 0.0001	-0.0164 ± 0.0001	0.0079 ± 0.0001	-0.0159 ± 0.0001	-0.0019 ± 0.0001	-0.0038 ± 0.0001
A_4	-0.0442 ± 0.0001	0.0883 ± 0.0001	-0.0443 ± 0.0001	0.0886 ± 0.0001	-0.0446 ± 0.0001	0.0893 ± 0.0001	-0.0432 ± 0.0001	0.0864 ± 0.0001	-0.0112 ± 0.0001	0.0224 ± 0.0002
A_5	0.1133 ± 0.0005	-0.2265 ± 0.0010	0.0949 ± 0.0004	-0.1899 ± 0.0007	0.1041 ± 0.0005	-0.2082 ± 0.0010	0.1173 ± 0.0005	-0.2346 ± 0.0010	0.0566 ± 0.0002	-0.1132 ± 0.0005
A_{6s}	-0.5509 ± 0.0026	0.9539 ± 0.0077	-0.5521 ± 0.0026	0.6915 ± 0.0056	-0.4374 ± 0.0022	0.9638 ± 0.0078	-0.6141 ± 0.0028	0.9325 ± 0.0076	-0.2392 ± 0.0023	0.3422 ± 0.0014
A_7	0.0000	-0.0130 ± 0.0001	-0.0130 ± 0.0001	-0.0260 ± 0.0001	-0.0095 ± 0.0001	-0.0190 ± 0.0001	-0.0011 ± 0.0001	-0.0022 ± 0.0001	-0.0062 ± 0.0001	-0.0124 ± 0.0001
A_8	0.0000	-0.0102 ± 0.0001	-0.0102 ± 0.0001	-0.0205 ± 0.0001	0.0000	0.0000	0.0000	0.0000	0.0000	0.0000
A_9	0.0000	-0.0042 ± 0.0001	-0.0042 ± 0.0001	-0.0083 ± 0.0001	0.0000	0.0000	0.0000	0.0000	0.0000	0.0000
$R_{D_s^*}$	0.2844 ± 0.0018		0.2842 ± 0.0018		0.2405 ± 0.0015		0.2486 ± 0.0016		0.2781 ± 0.0022	
A_{FB}^+	-0.0896 ± 0.0020		-0.0310 ± 0.0016		-0.1170 ± 0.0020		-0.0708 ± 0.0021		-0.0229 ± 0.0007	
A_{FB}^T	-0.3842 ± 0.0026		-0.2790 ± 0.0019		-0.3842 ± 0.0026		-0.3842 ± 0.0026		-0.1124 ± 0.0002	
$F_L^{P^*}$	0.4482 ± 0.0015		0.4493 ± 0.0015		0.4425 ± 0.0015		0.4606 ± 0.0015		0.3237 ± 0.0021	
C_F^I	-0.0550 ± 0.0014		-0.0558 ± 0.0014		-0.0555 ± 0.0014		-0.0537 ± 0.0014		-0.1316 ± 0.0004	

TABLE VII: Prediction of $B_s \rightarrow D_s^*(\rightarrow D_s\gamma, D_s\pi)\tau\nu$ decay observables in Scenerio - III.

In Fig 7 we show the q^2 and $\cos\theta_l$ dependence of various physical observables that exhibit same behaviour for the $D_s\gamma$ and $D_s\pi$ modes. NP contribution coming from g_{V_L} , g_{V_R} , g_{S_L} , g_{S_R} and g_{T_L} complex NP couplings are shown with blue, red, black, violet and orange colored lines, respectively. Our observations are as follows.

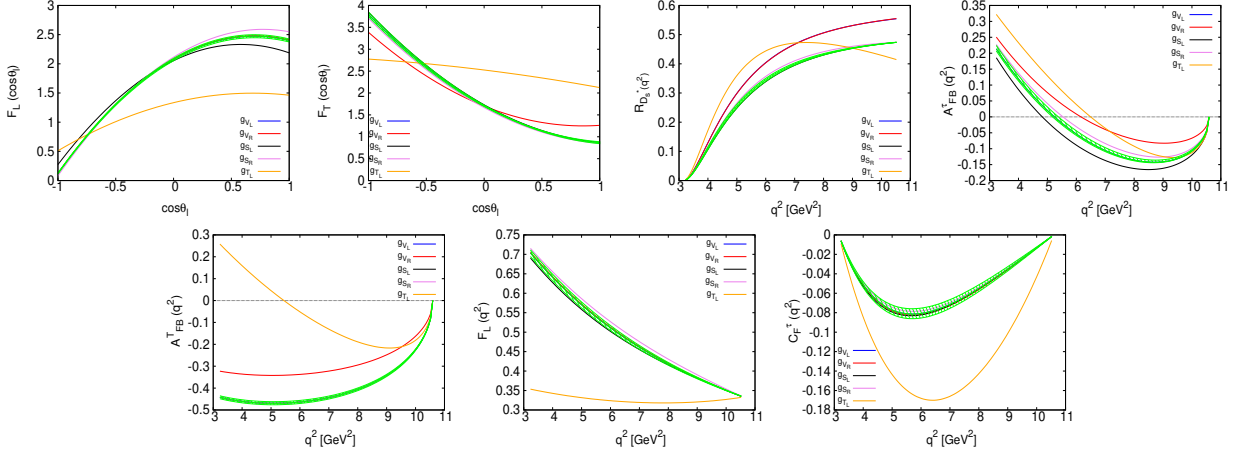


FIG. 7: The q^2 and $\cos\theta_l$ dependence of various physical observable of $B_s \rightarrow D_s^*(\rightarrow D_s\gamma, D_s\pi)\tau\nu$ in the SM and in the presence of the NP couplings of scenario - III. The SM central line and the corresponding error band are shown with green color. The blue, red, black, violet and orange colors represents the effect of NP coupling g_{V_L} , g_{V_R} , g_{S_L} , g_{S_R} and g_{T_L} respectively.

- In case of $F_L(\cos\theta_l)$, a significant deviation from the SM prediction is observed due to g_{T_L} NP coupling and it is quite distinct from the rest of NP couplings. Similarly, we observe significant deviation in $F_T(\cos\theta_l)$ once g_{V_R} and g_{T_L} NP couplings are switched on. Again, the behaviour of $F_T(\cos\theta_l)$ is quite distinct with g_{T_L} NP coupling.
- In case of $R_{D_s^*}(q^2)$, maximum deviation from the SM prediction is observed with g_{V_L} , g_{V_R} and g_{T_L} NP couplings and they are clearly distinguishable from the SM prediction. Although the shape of the q^2 distribution is quite similar for g_{V_L} and g_{V_R} couplings, it is, however, quite distinct for g_{T_L} NP coupling.
- In case of $A_{FB}^+(q^2)$, we observe a significant deviation from the SM due to g_{V_R} , g_{S_L} , g_{S_R} and g_{T_L} NP couplings. The zero crossing point is shifted to higher values of q^2 than in the SM for g_{V_R} , g_{S_R} and g_{T_L} , whereas, it is shifted to a low value of q^2 for g_{S_L} NP coupling. The observed zero crossings at $q^2 = 6.16\text{GeV}^2$, $q^2 = 4.82\text{GeV}^2$, $q^2 = 5.54\text{GeV}^2$ and $q^2 = 6.49\text{GeV}^2$ in the presence of g_{V_R} , g_{T_L} , g_{S_R} and g_{S_L} are clearly distinguishable from the SM zero crossing of $q^2 = 5.25 \pm 0.10\text{GeV}^2$ at the level of 9.1σ , 4.3σ , 2.9σ and 12σ significance.
- The observable $A_{FB}^T(q^2)$ shows a significant deviation from SM expectation once g_{V_R} and g_{T_L} NP couplings are switched on. We also observe a zero crossing in $A_{FB}^T(q^2)$ at $q^2 = 5.44\text{GeV}^2$ with g_{T_L} NP coupling. Similarly,

a significant deviation from the SM prediction is observed in $C_F^-(q^2)$ and $F_L(q^2)$ in the presence of g_{T_L} NP coupling. The dip in $C_F^-(q^2)$ is shifted to a higher value of q^2 than in the SM.

In Fig 8, we display q^2 and $\cos\theta_{D_s}$ dependence of several observable for $D_s\gamma$ (left panel) and $D_s\pi$ (right panel) modes. Our main observations are as follows.

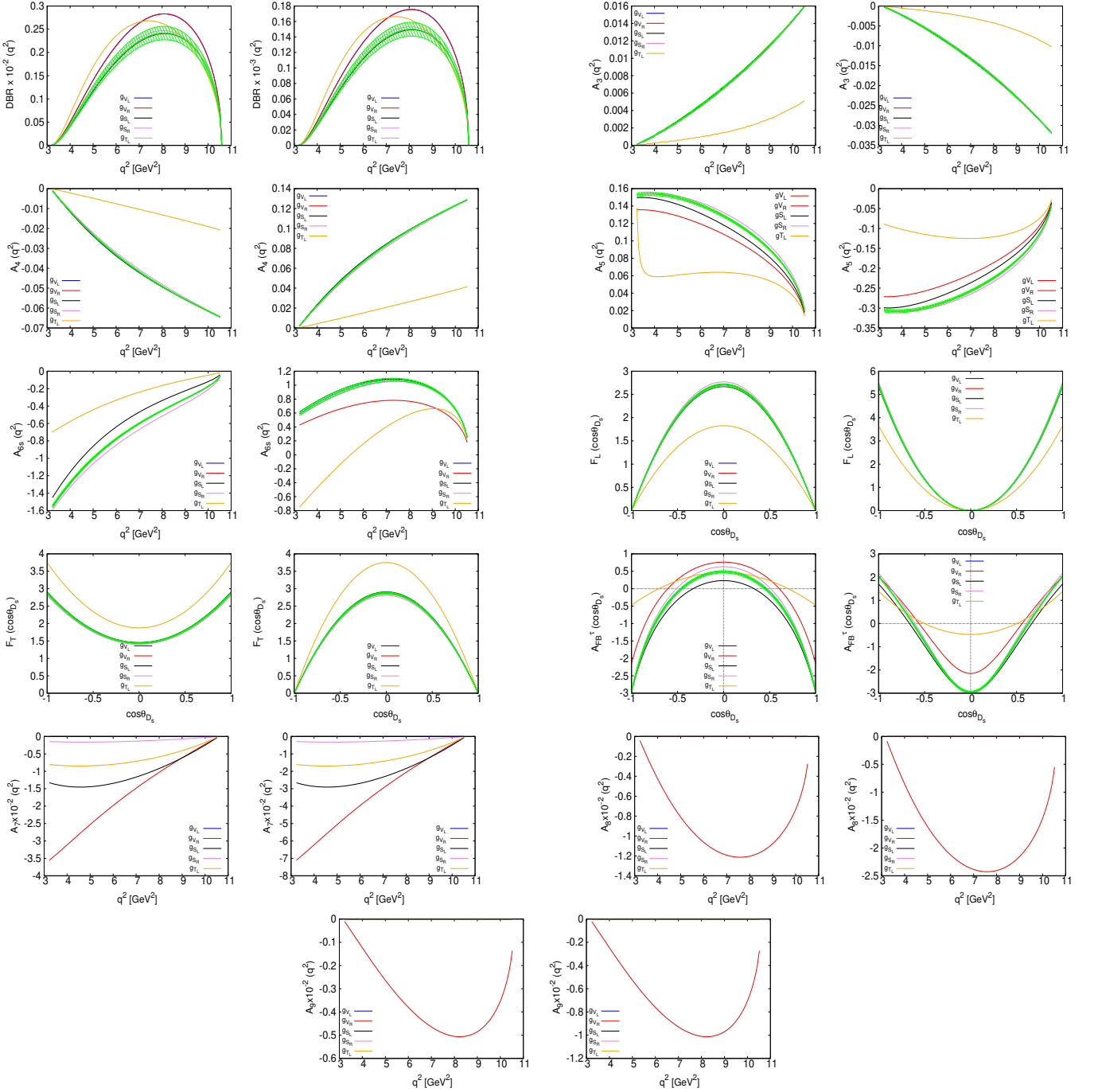


FIG. 8: The q^2 and $\cos\theta_{D_s}$ dependence of various physical observable of $B_s \rightarrow D_s^*(\rightarrow D_s\gamma, D_s\pi)\tau\nu$ in the SM and in the presence of the NP couplings of scenario - III. The SM central line and the corresponding error band are shown with green color. The blue, red, black, violet and orange colors represents the effect of NP couplings of g_{V_L} , g_{V_R} , g_{S_L} , g_{S_R} and g_{T_L} respectively.

- In case of $DBR(q^2)$, we observe significant deviation from the SM prediction with g_{T_L} , g_{V_L} and g_{V_R} NP couplings

for both $D_s\gamma$ and $D_s\pi$ modes. The peak of the distribution, however, is shifted to a low value of q^2 than in the SM with g_{T_L} NP coupling.

- The angular observable $A_3(q^2)$ and $A_4(q^2)$ show deviation from the SM in the presence of g_{T_L} NP coupling for both $D_s\gamma$ and $D_s\pi$ modes. Similarly, in case of $A_5(q^2)$, deviation from the SM prediction is observed in the presence of g_{V_R} , g_{S_L} and g_{T_L} NP coupling in both the decay modes. The deviation in $A_5(q^2)$, however, is more pronounced with g_{T_L} NP coupling.
- Deviation from the SM prediction in $A_{6s}(q^2)$ is observed with g_{S_L} , g_{S_R} and g_{T_L} NP couplings for the $D_s\gamma$ mode. The deviation is, however, more pronounced in case of g_{T_L} NP coupling. Similarly, for $D_s\pi$ mode, we see significant deviation in $A_{6s}(q^2)$ in the presence of g_{V_R} and g_{T_L} NP couplings. We also observe a zero crossing in the $A_{6s}(q^2)$ at $q^2 = 5.46\text{GeV}^2$ with g_{T_L} NP coupling.
- The $A_7(q^2)$ is non-zero with g_{V_R} , g_{S_L} , g_{S_R} and g_{T_L} NP couplings for both $D_s\gamma$ and $D_s\pi$ decay mode. Similar conclusions can be made for $D_s\pi$ mode as well because of the strict $A_7^\pi = 2A_7^\gamma$ relation.
- The angular observables $A_8(q^2)$ and $A_9(q^2)$ are non-zero only in the presence of g_{V_R} NP coupling for both $D_s\gamma$ and $D_s\pi$ modes. We observe a minimum of $A_8(q^2)$ and $A_9(q^2)$ at $q^2 = 7.5\text{GeV}^2$ and $q^2 = 8.28\text{GeV}^2$, respectively.
- Although a slight deviation in $F_L(\cos\theta_{D_s})$ and $F_T(\cos\theta_{D_s})$ is observed with g_{S_R} NP coupling, the deviation, however, is more pronounced with g_{T_L} NP coupling for both $D_s\gamma$ and $D_s\pi$ modes and it is clearly distinguishable from the SM prediction.
- Deviation from the SM prediction in $A_{FB}(\cos\theta_{D_s})$ is observed with g_{V_R} , g_{S_L} , g_{S_R} and g_{T_L} NP couplings for both $D_s\gamma$ and $D_s\pi$ modes. In the $D_s\gamma$ mode, we observe that the zero crossing in $A_{FB}(\cos\theta_{D_s})$ shifts to lower value of $\cos\theta_{D_s}$ than in the SM with g_{V_R} , g_{S_R} and g_{T_L} NP couplings, whereas, it shifts to a higher value of $\cos\theta_{D_s}$ with g_{S_L} NP coupling. The zero crossing points in $A_{FB}(\cos\theta_{D_s})$ at $\cos\theta_{D_s} = \pm 0.603, \pm 0.330, \pm 0.512$ and ± 0.703 in the presence of g_{V_R} , g_{S_L} , g_{S_R} and g_{T_L} NP couplings are clearly distinguishable from the SM zero crossing of $\cos\theta_{D_s} = \pm 0.454 \pm 0.018$ at $8.16\sigma, 7\sigma, 3.1\sigma$ and 13σ significance level, respectively. Similarly, for $D_s\pi$ mode, the zero crossing points in $A_{FB}(\cos\theta_{D_s})$ at $\cos\theta_{D_s} = \pm 0.558, \pm 0.663, \pm 0.604$ and ± 0.500 in the presence of these NP couplings are clearly distinguishable from the SM zero crossing of $\cos\theta_{D_s} = \pm 0.626 \pm 0.0075$ at $9\sigma, 4.9\sigma, 2.93\sigma$ and 16σ level of significance, respectively.

IV. CONCLUSIONS

Motivated by the anomalies present in several $b \rightarrow cl\nu$ quark level transition decays, we perform a detail angular analysis of $B_s \rightarrow D_s^*(\rightarrow D_s\gamma, D_s\pi)l\nu$ decays using the recent lattice QCD form factors. We use the latest global fit results of the possible NP couplings and estimate the effect of each NP couplings on several physical observables pertaining to $D_s\pi$ and $D_s\gamma$ modes in a model independent effective theory formalism.

We first report the SM results. In the SM, we obtain the branching ratio to be of $\mathcal{O}(10^{-2})$ for $D_s\gamma$ channel and $\mathcal{O}(10^{-3})$ for $D_s\pi$ channel. The LHCb collaboration reported the first measurement of the branching ratio to be $\mathcal{B}(B_s^0 \rightarrow D_s^{*-} \mu^+ \nu_\mu) = (5.38 \pm 0.25 \pm 0.46) \times 10^{-2}$ [95, 96] and it is in good agreement with our estimated results for the $D_s\gamma$ mode. The ratio of branching ratio is found to be $R_{D_s^*} = 0.2430 \pm 0.0015$ in the SM.

For our NP analysis we work with three different NP scenarios with the best fit values obtained from various recent global fit results. We assume both real and complex NP couplings in our analysis. We study the underlying observables based on NP contribution coming from single operators (1D) as well as from two different operators (2D). A brief summary of our results are as follows.

- In scenario - I, the observable $A_{FB}^\gamma(q^2)$ is found to be interesting as the zero crossing point observed with g_{S_L} and g_{S_R} and $g_{S_L} = 4g_{T_L}$ NP couplings stand at $1 - 2\sigma$ away from the SM zero crossing point. Similarly, the effect of g_{V_L} NP coupling is found to be prominent for $DBR(q^2)$ and $R_{D_s^*}(q^2)$.
- In scenerio-II, the deviation from the SM prediction observed for $DBR(q^2)$ and $R_{D_s^*}(q^2)$ is quite significant in the presence of $(g_{V_L}, g_{S_L} = -4g_{T_L})$ and (g_{V_L}, g_{S_R}) NP couplings. The zero crossings in $A_{FB}^\gamma(q^2)$ with (g_{S_R}, g_{S_L}) and $(g_{S_L} = 4g_{T_L})$ NP couplings are clearly distinguishable from the SM zero crossing point at more than 8σ and 10σ significance. Similarly, the zero crossing in $A_{FB}^\gamma(\cos\theta_{D_s})$ obtained with (g_{S_R}, g_{S_L}) and $(g_{S_L} = 4g_{T_L})$ NP couplings are distinguishable from the SM zero crossing at more than 7σ for both the $D_s\gamma$ mode and $D_s\pi$ mode. We find A_7 to be non-zero only in the presence of $g_{S_L} = 4g_{T_L}$ NP coupling.

- In scenario-III, the zero crossings in $A_{FB}^\tau(q^2)$ in the presence of g_{V_R} , g_{T_L} , g_{S_R} and g_{S_L} NP couplings are quite different from the SM zero crossing and they are clearly distinguishable from the SM prediction at the level of 9.1σ , 4.3σ , 2.9σ and 12σ significance. We also observe zero crossings in $A_{FB}^T(q^2)$ and $A_{6s}(q^2)$ with g_{T_L} NP coupling that are absent in the SM. The angular observable A_7 is found to be non-zero in the presence of g_{V_R} , g_{S_L} , g_{S_R} and g_{T_L} NP couplings, whereas, A_8 and A_9 are found to be non-zero only for g_{V_R} NP coupling. Moreover, the zero crossing points in $A_{FB}^\tau(\cos\theta_{D_s})$ obtained with g_{V_R} , g_{S_L} , g_{S_R} and g_{T_L} NP couplings are clearly distinguishable from the SM zero crossing at more than 8σ , 7σ , 3σ and 13σ significance level for the $D_s\gamma$ mode and they are distinguishable at more than 9σ , 4σ , 2σ and 15σ significance for the $D_s\pi$ mode. In general, the deviation from the SM prediction observed with complex tensor NP coupling g_{T_L} is more pronounced for all the observables in this scenario.

It should be noted that the angular observables $A_{FB}^\tau(q^2)$ and $A_{FB}^\tau(\cos\theta_{D_s})$ are quite interesting as they can be used to distinguish between several NP scenarios. Similarly, presence of zero crossings in $A_{FB}^T(q^2)$ and $A_{6s}(q^2)$ would be a clear signal of complex tensor NP coupling. Moreover, the angular observables A_7 , A_8 and A_9 will also play an important role in identifying the exact NP Lorentz structures. In conclusion, the results pertaining to $B_s \rightarrow D_s^*(\rightarrow D_s\gamma, D_s\pi) l\nu$ decay observables are very useful to explore ongoing flavor anomalies in $b \rightarrow cl\nu$ transitions and, in principle, it can provide us complementary information regarding NP in various B meson decays. At the same time, it can also be useful in determining the value of the CKM matrix element $|V_{cb}|$. Moreover, study of these decay modes both theoretically and experimentally can act as a useful ingredient in maximizing future sensitivity to NP.

-
- [1] J. A. Bailey *et al.* [MILC Collaboration], “ $B \rightarrow D l\nu$ form factors at nonzero recoil and $|V_{cb}|$ from 2+1-flavor lattice QCD,” Phys. Rev. D **92**, no. 3, 034506 (2015) doi:10.1103/PhysRevD.92.034506 [arXiv:1503.07237 [hep-lat]].
- [2] H. Na *et al.* [HPQCD Collaboration], “ $B \rightarrow D l\nu$ form factors at nonzero recoil and extraction of $|V_{cb}|$,” Phys. Rev. D **92**, no. 5, 054510 (2015) Erratum: [Phys. Rev. D **93**, no. 11, 119906 (2016)] doi:10.1103/PhysRevD.93.119906, 10.1103/PhysRevD.92.054510 [arXiv:1505.03925 [hep-lat]].
- [3] S. Aoki *et al.*, “Review of lattice results concerning low-energy particle physics,” Eur. Phys. J. C **77**, no. 2, 112 (2017) doi:10.1140/epjc/s10052-016-4509-7 [arXiv:1607.00299 [hep-lat]].
- [4] D. Bigi and P. Gambino, “Revisiting $B \rightarrow D l\nu$,” Phys. Rev. D **94**, no. 9, 094008 (2016) doi:10.1103/PhysRevD.94.094008 [arXiv:1606.08030 [hep-ph]].
- [5] F. U. Bernlochner, Z. Ligeti, M. Papucci and D. J. Robinson, Phys. Rev. D **95**, no.11, 115008 (2017) [erratum: Phys. Rev. D **97**, no.5, 059902 (2018)] doi:10.1103/PhysRevD.95.115008 [arXiv:1703.05330 [hep-ph]].
- [6] S. Jaiswal, S. Nandi and S. K. Patra, JHEP **12**, 060 (2017) doi:10.1007/JHEP12(2017)060 [arXiv:1707.09977 [hep-ph]].
- [7] B. Aubert *et al.* [BaBar], Phys. Rev. Lett. **104**, 011802 (2010) doi:10.1103/PhysRevLett.104.011802 [arXiv:0904.4063 [hep-ex]].
- [8] R. Glattauer *et al.* [Belle], Phys. Rev. D **93**, no.3, 032006 (2016) doi:10.1103/PhysRevD.93.032006 [arXiv:1510.03657 [hep-ex]].
- [9] J. P. Lees *et al.* [BaBar], “Evidence for an excess of $\bar{B} \rightarrow D^{(*)}\tau^-\bar{\nu}_\tau$ decays,” Phys. Rev. Lett. **109**, 101802 (2012) doi:10.1103/PhysRevLett.109.101802 [arXiv:1205.5442 [hep-ex]].
- [10] M. Huschle *et al.* [Belle], “Measurement of the branching ratio of $\bar{B} \rightarrow D^{(*)}\tau^-\bar{\nu}_\tau$ relative to $\bar{B} \rightarrow D^{(*)}\ell^-\bar{\nu}_\ell$ decays with hadronic tagging at Belle,” Phys. Rev. D **92**, no.7, 072014 (2015) doi:10.1103/PhysRevD.92.072014 [arXiv:1507.03233 [hep-ex]].
- [11] A. Abdesselam *et al.* [Belle Collaboration], “Measurement of $\mathcal{R}(D)$ and $\mathcal{R}(D^*)$ with a semileptonic tagging method,” arXiv:1904.08794 [hep-ex].
- [12] S. Fajfer, J. F. Kamenik and I. Nisandzic, Phys. Rev. D **85**, 094025 (2012) doi:10.1103/PhysRevD.85.094025 [arXiv:1203.2654 [hep-ph]].
- [13] D. Bigi, P. Gambino and S. Schacht, JHEP **11**, 061 (2017) doi:10.1007/JHEP11(2017)061 [arXiv:1707.09509 [hep-ph]].
- [14] C. Bernard *et al.*, “The $\bar{B} \rightarrow D^*\ell\bar{\nu}$ form factor at zero recoil from three-flavor lattice QCD: A Model independent determination of $|V_{cb}|$,” Phys. Rev. D **79**, 014506 (2009) doi:10.1103/PhysRevD.79.014506 [arXiv:0808.2519 [hep-lat]].
- [15] J. A. Bailey *et al.* [Fermilab Lattice and MILC Collaborations], “Update of $|V_{cb}|$ from the $\bar{B} \rightarrow D^*\ell\bar{\nu}$ form factor at zero recoil with three-flavor lattice QCD,” Phys. Rev. D **89**, no. 11, 114504 (2014) doi:10.1103/PhysRevD.89.114504 [arXiv:1403.0635 [hep-lat]].
- [16] J. P. Lees *et al.* [BaBar], Phys. Rev. D **88**, no.7, 072012 (2013) doi:10.1103/PhysRevD.88.072012 [arXiv:1303.0571 [hep-ex]].
- [17] S. Hirose *et al.* [Belle], Phys. Rev. Lett. **118**, no.21, 211801 (2017) doi:10.1103/PhysRevLett.118.211801 [arXiv:1612.00529 [hep-ex]].
- [18] S. Hirose *et al.* [Belle], Phys. Rev. D **97**, no.1, 012004 (2018) doi:10.1103/PhysRevD.97.012004 [arXiv:1709.00129 [hep-ex]].
- [19] R. Aaij *et al.* [LHCb], “Measurement of the ratio of branching fractions $\mathcal{B}(\bar{B}^0 \rightarrow D^{*+}\tau^-\bar{\nu}_\tau)/\mathcal{B}(\bar{B}^0 \rightarrow D^{*+}\mu^-\bar{\nu}_\mu)$,” Phys. Rev. Lett. **115**, no.11, 111803 (2015) [erratum: Phys. Rev. Lett. **115**, no.15, 159901 (2015)] doi:10.1103/PhysRevLett.115.111803 [arXiv:1506.08614 [hep-ex]].

- [20] R. Aaij *et al.* [LHCb], Phys. Rev. D **97**, no.7, 072013 (2018) doi:10.1103/PhysRevD.97.072013 [arXiv:1711.02505 [hep-ex]].
- [21] A. Abdesselam *et al.* [Belle], [arXiv:1904.08794 [hep-ex]].
- [22] M. A. Ivanov, J. G. Korner and P. Santorelli, “The Semileptonic decays of the B_c meson,” Phys. Rev. D **63**, 074010 (2001) doi:10.1103/PhysRevD.63.074010 [hep-ph/0007169].
- [23] D. Ebert, R. N. Faustov and V. O. Galkin, “Weak decays of the B_c meson to charmonium and D mesons in the relativistic quark model,” Phys. Rev. D **68**, 094020 (2003) doi:10.1103/PhysRevD.68.094020 [hep-ph/0306306].
- [24] A. Abd El-Hady, J. H. Munoz and J. P. Vary, “Semileptonic and nonleptonic $B(c)$ decays,” Phys. Rev. D **62**, 014019 (2000) doi:10.1103/PhysRevD.62.014019 [hep-ph/9909406].
- [25] W. F. Wang, Y. Y. Fan and Z. J. Xiao, “Semileptonic decays $B_c \rightarrow (\eta_c, J/\Psi)l\nu$ in the perturbative QCD approach,” Chin. Phys. C **37**, 093102 (2013) doi:10.1088/1674-1137/37/9/093102 [arXiv:1212.5903 [hep-ph]].
- [26] Y. K. Hsiao and C. Q. Geng, “Branching fractions of $B_{(c)}$ decays involving J/ψ and $X(3872)$,” Chin. Phys. C **41**, no. 1, 013101 (2017) doi:10.1088/1674-1137/41/1/013101 [arXiv:1607.02718 [hep-ph]].
- [27] R. Dutta and A. Bhol, “ $B_c \rightarrow (J/\psi, \eta_c)\tau\nu$ semileptonic decays within the standard model and beyond,” Phys. Rev. D **96**, no. 7, 076001 (2017) doi:10.1103/PhysRevD.96.076001 [arXiv:1701.08598 [hep-ph]].
- [28] R. Dutta, “Exploring R_D, R_{D^*} and $R_{J/\psi}$ anomalies,” arXiv:1710.00351 [hep-ph].
- [29] T. D. Cohen, H. Lamm and R. F. Lebed, “Model-independent bounds on $R(J/\psi)$,” JHEP **1809**, 168 (2018) doi:10.1007/JHEP09(2018)168 [arXiv:1807.02730 [hep-ph]].
- [30] J. Harrison *et al.* [HPQCD], Phys. Rev. D **102**, no.9, 094518 (2020) doi:10.1103/PhysRevD.102.094518 [arXiv:2007.06957 [hep-lat]].
- [31] S. Hirose *et al.* [Belle Collaboration], “Measurement of the τ lepton polarization and $R(D^*)$ in the decay $\bar{B} \rightarrow D^*\tau^-\bar{\nu}_\tau$,” Phys. Rev. Lett. **118**, no. 21, 211801 (2017) doi:10.1103/PhysRevLett.118.211801 [arXiv:1612.00529 [hep-ex]].
- [32] S. Hirose *et al.* [Belle Collaboration], “Measurement of the τ lepton polarization and $R(D^*)$ in the decay $\bar{B} \rightarrow D^*\tau^-\bar{\nu}_\tau$ with one-prong hadronic τ decays at Belle,” Phys. Rev. D **97**, no. 1, 012004 (2018) doi:10.1103/PhysRevD.97.012004 [arXiv:1709.00129 [hep-ex]].
- [33] M. Tanaka and R. Watanabe, “New physics in the weak interaction of $\bar{B} \rightarrow D^{(*)}\tau\bar{\nu}$,” Phys. Rev. D **87**, no. 3, 034028 (2013) doi:10.1103/PhysRevD.87.034028 [arXiv:1212.1878 [hep-ph]].
- [34] A. Abdesselam *et al.* [Belle Collaboration], “Measurement of the D^{*-} polarization in the decay $B^0 \rightarrow D^{*-}\tau^+\nu_\tau$,” arXiv:1903.03102 [hep-ex].
- [35] A. K. Alok, D. Kumar, S. Kumbhakar and S. U. Sankar, “ D^* polarization as a probe to discriminate new physics in $\bar{B} \rightarrow D^*\tau\bar{\nu}$,” Phys. Rev. D **95**, no. 11, 115038 (2017) doi:10.1103/PhysRevD.95.115038 [arXiv:1606.03164 [hep-ph]].
- [36] Y. Sakaki, M. Tanaka, A. Tayduganov and R. Watanabe, “Probing New Physics with q^2 distributions in $\bar{B} \rightarrow D^{(*)}\tau\bar{\nu}$,” Phys. Rev. D **91**, no. 11, 114028 (2015) doi:10.1103/PhysRevD.91.114028 [arXiv:1412.3761 [hep-ph]].
- [37] P. Biancofiore, P. Colangelo and F. De Fazio, “On the anomalous enhancement observed in $B \rightarrow D\tau\bar{\nu}$ decays,” Phys. Rev. D **87**, no. 7, 074010 (2013) doi:10.1103/PhysRevD.87.074010 [arXiv:1302.1042 [hep-ph]].
- [38] M. Freytsis, Z. Ligeti and J. T. Ruderman, “Flavor models for $\bar{B} \rightarrow D^{(*)}\tau\bar{\nu}$,” Phys. Rev. D **92**, no. 5, 054018 (2015) doi:10.1103/PhysRevD.92.054018 [arXiv:1506.08896 [hep-ph]].
- [39] R. Dutta, “ $\Lambda_b \rightarrow (\Lambda_c, p)\tau\nu$ decays within standard model and beyond,” Phys. Rev. D **93**, no. 5, 054003 (2016) doi:10.1103/PhysRevD.93.054003 [arXiv:1512.04034 [hep-ph]].
- [40] S. Bhattacharya, S. Nandi and S. K. Patra, “Looking for possible new physics in $B \rightarrow D^{(*)}\tau\nu$ in light of recent data,” Phys. Rev. D **95**, no. 7, 075012 (2017) doi:10.1103/PhysRevD.95.075012 [arXiv:1611.04605 [hep-ph]].
- [41] P. Colangelo and F. De Fazio, “Tension in the inclusive versus exclusive determinations of $|V_{cb}|$: a possible role of new physics,” Phys. Rev. D **95**, no. 1, 011701 (2017) doi:10.1103/PhysRevD.95.011701 [arXiv:1611.07387 [hep-ph]].
- [42] R. Dutta and A. Bhol, “ $b \rightarrow (c, u)\tau\nu$ leptonic and semileptonic decays within an effective field theory approach,” Phys. Rev. D **96**, no. 3, 036012 (2017) doi:10.1103/PhysRevD.96.036012 [arXiv:1611.00231 [hep-ph]].
- [43] A. K. Alok, D. Kumar, J. Kumar, S. Kumbhakar and S. U. Sankar, “New physics solutions for R_D and R_{D^*} ,” JHEP **1809**, 152 (2018) doi:10.1007/JHEP09(2018)152 [arXiv:1710.04127 [hep-ph]].
- [44] A. Azatov, D. Bardhan, D. Ghosh, F. Sgarlata and E. Venturini, “Anatomy of $b \rightarrow c\tau\nu$ anomalies,” JHEP **1811**, 187 (2018) doi:10.1007/JHEP11(2018)187 [arXiv:1805.03209 [hep-ph]].
- [45] S. Bifani, S. Descotes-Genon, A. Romero Vidal and M. H. Schune, “Review of Lepton Universality tests in B decays,” J. Phys. G **46**, no. 2, 023001 (2019) doi:10.1088/1361-6471/aaf5de [arXiv:1809.06229 [hep-ex]].
- [46] Z. R. Huang, Y. Li, C. D. Lu, M. A. Paracha and C. Wang, “Footprints of New Physics in $b \rightarrow c\tau\nu$ Transitions,” Phys. Rev. D **98**, no. 9, 095018 (2018) doi:10.1103/PhysRevD.98.095018 [arXiv:1808.03565 [hep-ph]].
- [47] Q. Y. Hu, X. Q. Li and Y. D. Yang, “ $b \rightarrow c\tau\nu$ transitions in the standard model effective field theory,” Eur. Phys. J. C **79**, no. 3, 264 (2019) doi:10.1140/epjc/s10052-019-6766-8 [arXiv:1810.04939 [hep-ph]].
- [48] F. Feruglio, P. Paradisi and O. Sumensari, “Implications of scalar and tensor explanations of $R_{D^{(*)}}$,” JHEP **1811**, 191 (2018) doi:10.1007/JHEP11(2018)191 [arXiv:1806.10155 [hep-ph]].
- [49] M. Jung and D. M. Straub, “Constraining new physics in $b \rightarrow c\ell\nu$ transitions,” JHEP **1901**, 009 (2019) doi:10.1007/JHEP01(2019)009 [arXiv:1801.01112 [hep-ph]].
- [50] A. Datta, S. Kamali, S. Meinel and A. Rashed, “Phenomenology of $\Lambda_b \rightarrow \Lambda_c\tau\bar{\nu}_\tau$ using lattice QCD calculations,” JHEP **1708**, 131 (2017) doi:10.1007/JHEP08(2017)131 [arXiv:1702.02243 [hep-ph]].
- [51] F. U. Bernlochner, Z. Ligeti, D. J. Robinson and W. L. Sutcliffe, “New predictions for $\Lambda_b \rightarrow \Lambda_c$ semileptonic decays and tests of heavy quark symmetry,” Phys. Rev. Lett. **121**, no. 20, 202001 (2018) doi:10.1103/PhysRevLett.121.202001 [arXiv:1808.09464 [hep-ph]].

- [52] A. K. Alok, D. Kumar, S. Kumbhakar and S. Uma Sankar, “Resolution of R_D/R_{D^*} puzzle,” Phys. Lett. B **784**, 16 (2018) doi:10.1016/j.physletb.2018.07.001 [arXiv:1804.08078 [hep-ph]].
- [53] R. Dutta, “Phenomenology of $\Xi_b \rightarrow \Xi_c \tau \nu$ decays,” Phys. Rev. D **97**, no. 7, 073004 (2018) doi:10.1103/PhysRevD.97.073004 [arXiv:1801.02007 [hep-ph]].
- [54] R. Dutta and N. Rajeev, “Signature of lepton flavor universality violation in $B_s \rightarrow D_s \tau \nu$ semileptonic decays,” Phys. Rev. D **97**, no. 9, 095045 (2018) doi:10.1103/PhysRevD.97.095045 [arXiv:1803.03038 [hep-ph]].
- [55] S. Fajfer, J. F. Kamenik, I. Nisandzic and J. Zupan, “Implications of Lepton Flavor Universality Violations in B Decays,” Phys. Rev. Lett. **109**, 161801 (2012) doi:10.1103/PhysRevLett.109.161801 [arXiv:1206.1872 [hep-ph]].
- [56] A. Crivellin, C. Greub and A. Kokulu, “Explaining $B \rightarrow D \tau \nu$, $B \rightarrow D^* \tau \nu$ and $B \rightarrow \tau \nu$ in a 2HDM of type III,” Phys. Rev. D **86**, 054014 (2012) doi:10.1103/PhysRevD.86.054014 [arXiv:1206.2634 [hep-ph]].
- [57] X. Q. Li, Y. D. Yang and X. Zhang, “Revisiting the one leptoquark solution to the $R_{D^{(*)}}$ anomalies and its phenomenological implications,” JHEP **1608**, 054 (2016) doi:10.1007/JHEP08(2016)054 [arXiv:1605.09308 [hep-ph]].
- [58] B. Bhattacharya, A. Datta, J. P. Guévin, D. London and R. Watanabe, “Simultaneous Explanation of the R_K and $R_{D^{(*)}}$ Puzzles: a Model Analysis,” JHEP **1701**, 015 (2017) doi:10.1007/JHEP01(2017)015 [arXiv:1609.09078 [hep-ph]].
- [59] D. Leljak and B. Melic, “ $|V_{ub}|$ determination and testing of lepton flavour universality in semileptonic $B_c \rightarrow D^{(*)}$ decays,” arXiv:1909.01213 [hep-ph].
- [60] D. Bečirević, M. Fedele, I. Nišandžić and A. Tayduganov, “Lepton Flavor Universality tests through angular observables of $\bar{B} \rightarrow D^{(*)} \ell \bar{\nu}$ decay modes,” arXiv:1907.02257 [hep-ph].
- [61] N. Rajeev and R. Dutta, “Impact of vector new physics couplings on $B_s \rightarrow (K, K^*) \tau \nu$ and $B \rightarrow \pi \tau \nu$ decays,” Phys. Rev. D **98**, no. 5, 055024 (2018) doi:10.1103/PhysRevD.98.055024 [arXiv:1808.03790 [hep-ph]].
- [62] R. Dutta, “Predictions of $B_c \rightarrow (D, D^*) \tau \nu$ decay observables in the standard model,” J. Phys. G **46**, no. 3, 035008 (2019) doi:10.1088/1361-6471/ab0059 [arXiv:1809.08561 [hep-ph]].
- [63] P. Colangelo and F. De Fazio, “Scrutinizing $\bar{B} \rightarrow D^* (D\pi) \ell^- \bar{\nu}_\ell$ and $\bar{B} \rightarrow D^* (D\gamma) \ell^- \bar{\nu}_\ell$ in search of new physics footprints,” JHEP **1806**, 082 (2018) doi:10.1007/JHEP06(2018)082 [arXiv:1801.10468 [hep-ph]].
- [64] D. Bardhan, P. Byakti and D. Ghosh, “A closer look at the R_D and R_{D^*} anomalies,” JHEP **1701**, 125 (2017) doi:10.1007/JHEP01(2017)125 [arXiv:1610.03038 [hep-ph]].
- [65] Y. Li and C. D. Lü, “Recent Anomalies in B Physics,” Sci. Bull. **63**, 267 (2018) doi:10.1016/j.scib.2018.02.003 [arXiv:1808.02990 [hep-ph]].
- [66] J. D. Gómez, N. Quintero and E. Rojas, “Charged current $b \rightarrow c \tau \bar{\nu}_\tau$ anomalies in a general W' boson scenario,” arXiv:1907.08357 [hep-ph].
- [67] A. K. Alok, D. Kumar, S. Kumbhakar and S. Uma Sankar, “New Physics solutions for $b \rightarrow c \tau \bar{\nu}$ anomalies before and after Moriond 2019,” arXiv:1903.10486 [hep-ph].
- [68] N. Rajeev, R. Dutta and S. Kumbhakar, “Implication of $R_{D^{(*)}}$ anomalies on semileptonic decays of Σ_b and Ω_b baryons,” Phys. Rev. D **100**, no. 3, 035015 (2019) doi:10.1103/PhysRevD.100.035015 [arXiv:1905.13468 [hep-ph]].
- [69] R. Dutta, “Model independent analysis of new physics effects on $B_c \rightarrow (D_s, D_s^*) \mu^+ \mu^-$ decay observables,” Phys. Rev. D **100**, no. 7, 075025 (2019) doi:10.1103/PhysRevD.100.075025 [arXiv:1906.02412 [hep-ph]].
- [70] H. Yan, Y. D. Yang and X. B. Yuan, “Phenomenology of $b \rightarrow c \tau \bar{\nu}$ decays in a scalar leptoquark model,” Chin. Phys. C **43**, no. 8, 083105 (2019) doi:10.1088/1674-1137/43/8/083105 [arXiv:1905.01795 [hep-ph]].
- [71] O. Popov, M. A. Schmidt and G. White, “ R_2 as a single leptoquark solution to $R_{D^{(*)}}$ and $R_{K^{(*)}}$,” Phys. Rev. D **100**, no. 3, 035028 (2019) doi:10.1103/PhysRevD.100.035028 [arXiv:1905.06339 [hep-ph]].
- [72] K. Azizi, Y. Sarac and H. Sundu, “Lepton flavor universality violation in semileptonic tree level weak transitions,” Phys. Rev. D **99**, no. 11, 113004 (2019) doi:10.1103/PhysRevD.99.113004 [arXiv:1904.08267 [hep-ph]].
- [73] X. L. Mu, Y. Li, Z. T. Zou and B. Zhu, “Investigation of Effects of New Physics in $\Lambda_b \rightarrow \Lambda_c \tau \bar{\nu}_\tau$ Decay,” Phys. Rev. D **100**, no. 11, 113004 (2019) doi:10.1103/PhysRevD.100.113004 [arXiv:1909.10769 [hep-ph]].
- [74] K. Azizi, A. T. Olgun and Z. Tavukoglu, “Effects of vector leptoquarks on $\Lambda_b \rightarrow \Lambda_c \ell \bar{\nu}_\ell$ decay,” arXiv:1912.03007 [hep-ph].
- [75] P. Colangelo, F. De Fazio and F. Loporco, “Probing New Physics with $\bar{B} \rightarrow \rho(770) \ell^- \bar{\nu}_\ell$ and $\bar{B} \rightarrow a_1(1260) \ell^- \bar{\nu}_\ell$,” Phys. Rev. D **100**, no. 7, 075037 (2019) doi:10.1103/PhysRevD.100.075037 [arXiv:1906.07068 [hep-ph]].
- [76] W. Altmannshofer, P. S. Bhupal Dev and A. Soni, “ $R_{D^{(*)}}$ anomaly: A possible hint for natural supersymmetry with R -parity violation,” Phys. Rev. D **96**, no. 9, 095010 (2017) doi:10.1103/PhysRevD.96.095010 [arXiv:1704.06659 [hep-ph]].
- [77] Z. Rui, H. Li, G. x. Wang and Y. Xiao, “Semileptonic decays of B_c meson to S-wave charmonium states in the perturbative QCD approach,” Eur. Phys. J. C **76**, no. 10, 564 (2016) doi:10.1140/epjc/s10052-016-4424-y [arXiv:1602.08918 [hep-ph]].
- [78] M. Blanke, A. Crivellin, S. de Boer, T. Kitahara, M. Moscati, U. Nierste and I. Nišandžić, “Impact of polarization observables and $B_c \rightarrow \tau \nu$ on new physics explanations of the $b \rightarrow c \tau \nu$ anomaly,” Phys. Rev. D **99** (2019) no.7, 075006 [arXiv:1811.09603 [hep-ph]].
- [79] M. Blanke, A. Crivellin, T. Kitahara, M. Moscati, U. Nierste and I. Nišandžić, Phys. Rev. D **100** (2019) no.3, 035035 [arXiv:1905.08253 [hep-ph]].
- [80] C. Murgui, A. Peñuelas, M. Jung and A. Pich, “Global fit to $b \rightarrow c \tau \nu$ transitions,” JHEP **09**, 103 (2019) doi:10.1007/JHEP09(2019)103 [arXiv:1904.09311 [hep-ph]].
- [81] S. M. Zhao, X. Liu and S. J. Li, “Study on $B(s) \rightarrow_l D(s) l$ anti- ν Semileptonic Decays in the CQM Model,” Eur. Phys. J. C **51**, 601 (2007) doi:10.1140/epjc/s10052-007-0322-7 [hep-ph/0612008].
- [82] K. Azizi and M. Bayar, “Semileptonic $B(q) \rightarrow_l D^*(q) l \nu$ ($q=s, d, u$) Decays in QCD Sum Rules,” Phys. Rev. D **78**, 054011 (2008) doi:10.1103/PhysRevD.78.054011 [arXiv:0806.0578 [hep-ph]].

- [83] M. Bayar and K. Azizi, “Semileptonic $B(q) \rightarrow D^*(q)l\nu$ ($q=s, d, u$) transitions in QCD,” Nucl. Phys. Proc. Suppl. **186**, 395 (2009) doi:10.1016/j.nuclphysbps.2008.12.089 [arXiv:0809.3866 [hep-ph]].
- [84] R. H. Li, C. D. Lu and Y. M. Wang, “Exclusive $B(s)$ decays to the charmed mesons $D(s) + (1968, 2317)$ in the standard model,” Phys. Rev. D **80**, 014005 (2009) doi:10.1103/PhysRevD.80.014005 [arXiv:0905.3259 [hep-ph]].
- [85] M. Bordone, N. Gubernari, D. van Dyk and M. Jung, “Heavy-Quark Expansion for $\bar{B}_s \rightarrow D_s^{(*)}$ Form Factors and Unitarity Bounds beyond the $SU(3)_F$ Limit,” arXiv:1912.09335 [hep-ph].
- [86] G. Li, F. I. Shao and W. Wang, “ $B_s \rightarrow D_s(3040)$ form factors and B_s decays into $D_s(3040)$,” Phys. Rev. D **82**, 094031 (2010) doi:10.1103/PhysRevD.82.094031 [arXiv:1008.3696 [hep-ph]].
- [87] X. J. Chen, H. F. Fu, C. S. Kim and G. L. Wang, “Estimating Form Factors of $B_s \rightarrow D_s^{(*)}$ and their Applications to Semileptonic and Non-leptonic Decays,” J. Phys. G **39**, 045002 (2012) doi:10.1088/0954-3899/39/4/045002 [arXiv:1106.3003 [hep-ph]].
- [88] T. Zhou, T. h. Wang, Y. Jiang, X. Z. Tan, G. Li and G. L. Wang, “Relativistic calculations of $R(D^{(*)})$, $R(D_s^{(*)})$, $R(\eta_c)$ and $R(J/\psi)$,” arXiv:1910.06595 [hep-ph].
- [89] J. Harrison *et al.* [HPQCD Collaboration], “Lattice QCD calculation of the $B_{(s)} \rightarrow D_{(s)}^* \ell \nu$ form factors at zero recoil and implications for $|V_{cb}|$,” Phys. Rev. D **97**, no. 5, 054502 (2018) doi:10.1103/PhysRevD.97.054502 [arXiv:1711.11013 [hep-lat]].
- [90] Y. Y. Fan, W. F. Wang and Z. J. Xiao, “Study of $\bar{B}_s^0 \rightarrow (D_s^+, D_s^{*+}) l^- \bar{\nu}_l$ decays in the pQCD factorization approach,” Phys. Rev. D **89**, no. 1, 014030 (2014) doi:10.1103/PhysRevD.89.014030 [arXiv:1311.4965 [hep-ph]].
- [91] S. Sahoo and R. Mohanta, “Investigating the role of new physics in $b \rightarrow c\tau\bar{\nu}_\tau$ transitions,” arXiv:1910.09269 [hep-ph].
- [92] T. D. Cohen, H. Lamm and R. F. Lebed, “Precision Model-Independent Bounds from Global Analysis of $b \rightarrow c\ell\nu$ Form Factors,” arXiv:1909.10691 [hep-ph].
- [93] R. N. Faustov and V. O. Galkin, “Weak decays of B_s mesons to D_s mesons in the relativistic quark model,” Phys. Rev. D **87**, no. 3, 034033 (2013) doi:10.1103/PhysRevD.87.034033 [arXiv:1212.3167 [hep-ph]].
- [94] N. Das and R. Dutta, “Implication of $b \rightarrow c\tau\nu$ flavor anomalies on $B_s \rightarrow D_s^* \tau\nu$ decay observables,” J. Phys. G **47**, no.11, 115001 (2020) doi:10.1088/1361-6471/aba422 [arXiv:1912.06811 [hep-ph]].
- [95] R. Aaij *et al.* [LHCb], “Measurement of $|V_{cb}|$ with $B_s^0 \rightarrow D_s^{(*)-} \mu^+ \nu_\mu$ decays,” Phys. Rev. D **101**, no.7, 072004 (2020) doi:10.1103/PhysRevD.101.072004 [arXiv:2001.03225 [hep-ex]].
- [96] R. Aaij *et al.* [LHCb], “Measurement of the shape of the $B_s^0 \rightarrow D_s^{*-} \mu^+ \nu_\mu$ differential decay rate,” [arXiv:2003.08453 [hep-ex]].
- [97] P.A. Zyla *et al.* [Particle Data Group], PTEP **2020**, no.8, 083C01 (2020) doi:10.1093/ptep/ptaa104
- [98] J. Harrison *et al.* [LATTICE-HPQCD], “ $B_s \rightarrow D_s^*$ Form Factors for the full q^2 range from Lattice QCD,” [arXiv:2105.11433 [hep-lat]].
- [99] T. Bhattacharya, V. Cirigliano, S. D. Cohen, A. Filipuzzi, M. Gonzalez-Alonso, M. L. Graesser, R. Gupta and H. W. Lin, “Probing Novel Scalar and Tensor Interactions from (Ultra)Cold Neutrons to the LHC,” Phys. Rev. D **85**, 054512 (2012) doi:10.1103/PhysRevD.85.054512 [arXiv:1110.6448 [hep-ph]].
- [100] V. Cirigliano, J. Jenkins and M. Gonzalez-Alonso, “Semileptonic decays of light quarks beyond the Standard Model,” Nucl. Phys. B **830**, 95 (2010) doi:10.1016/j.nuclphysb.2009.12.020 [arXiv:0908.1754 [hep-ph]].
- [101] P. Colangelo, F. De Fazio and F. Loporco, “Role of $B_c^+ \rightarrow B_{s,d}^{(*)} \bar{\ell} \nu_\ell$ in the Standard Model and in the search for BSM signals,” Phys. Rev. D **103**, no.7, 075019 (2021) doi:10.1103/PhysRevD.103.075019 [arXiv:2102.05365 [hep-ph]].
- [102] R. Mandal, C. Murgui, A. Peñuelas and A. Pich, “The role of right-handed neutrinos in $b \rightarrow c\tau\bar{\nu}$ anomalies,” JHEP **08**, no.08, 022 (2020) doi:10.1007/JHEP08(2020)022 [arXiv:2004.06726 [hep-ph]].